Analysis of Multiform Optical Solitons Structures for a Dual-Mode Nonlinear Schrödinger Model under Square Root Kerr Law

Mati ur Rahman[1], **Sonia Akram** [2], **Laila A. AL-Essa** [3*]

[1]*Department of Mathematics, Faculty of Science, University of Gujrat, Gujrat-50700, Pakistan*

[2] *Department of Mathematics and Statistics, College of Sciences, Imam Mohammad Ibn Saud Islamic University (IMSIU), Riyadh, Saudi Arabia.*

[3]*Department of Mathematical Sciences, College of Science, Princess Nourah bint Abdulrahman University, P.O.Box 84428, Riyadh 11671, Saudi Arabia.*

Abstract

This study investigates a novel dual-mode resonant nonlinear Schrödinger equation (RNLSE) incorporating the Bohm potential and governed by the square root Kerr law, a physically significant nonlinearity arising in nonlinear optics and quantum fluids. Motivated by applications in fiber communication, optical pulse propagation, and nonlinear engineering systems, we utilize two powerful analytical approaches: the enhanced modified extended tanh function method (eMETFM) and the $\left(\frac{\mathcal{G}'}{\mathcal{G}^2}\right)$-expansion method. These techniques are utilized to obtain a variety of exact wave solutions to the governing RNLSE. The solutions obtained include hyperbolic, trigonometric, and rational forms, each capturing distinct physical regimes and wave structures relevant to dual-mode optical systems. The implementation of a suitable wave transformation reduces the RNLSE into ordinary differential form, facilitating the application of the respective methods. To demonstrate the behavior of the resulting solitonic solutions, we present 2D plots, 3D surface visualizations, and contour projections. These graphical interpretations reveal different solitary wave patterns and amplitude profiles, showcasing their stability and structural dynamics. The results not only emphasize the rich wave phenomena inherent in the considered dual-mode system but also confirm the applicability and reliability of the proposed techniques for analyzing nonlinear wave equations in advanced physical and engineering contexts. The outcomes are expected to contribute meaningfully to the modeling and design of devices in laser systems, fiber optics, and quantum communication channels.

Keywords: Dual-mode resonant nonlinear Schrödinger equation; Bohm potential; Square root Kerr law; Optical solitons; enhanced modified extended tanh function method; $\left(\frac{\mathcal{G}'}{\mathcal{G}^2}\right)$-expansion method

1. Introduction

Nonlinear partial differential equations (NLPDEs) serve as a basic framework for modeling a vast array of complex physical, biological, and engineering systems [1, 2]. Their importance lies in their ability to elaborate phenomena where linear approximations fail to capture the essential dynamics, specifically when nonlinear interactions and wave dispersion play critical roles. NLPDEs are instrumental in understanding wave propagation, soliton dynamics, pattern formation, and chaotic behavior in different fields such as fluid dynamics, plasma physics, nonlinear optics, quantum mechanics,

Email addresses: mrmahman@imamu.edu.sa (Mati ur Rahman[1]), soniaakram641@gmal.com (Sonia Akram [2]), Laalessa@pnu.edu.sa (Laila A. AL-Essa [3*])

population biology, chemical kinetics, and neuroscience [3, 4]. In contrast to linear models, NLPDEs can support rich solution structures including solitary waves, blow-up phenomena, and bifurcation patterns, which relate to real-world behaviors observed in experiments and applications [5, 6]. Additionally, advances in analytical and computational techniques for solving NLPDEs continue to drive innovation in both theoretical research and technological development, particularly in areas like fiber-optic communication, metamaterials, and nonlinear control systems [7, 8, 9, 10].

Despite their utility, one of the major challenges in working with NLPDEs lies in determining exact analytical solutions, specifically when dealing with highly nonlinear or fractional-order models. To overcome this, numerous analytical techniques have been presented, such as the generalized Kudryashov method [11], extended trial equation technique [12], exp-function method [13], He's semi-inverse approach [14], and various auxiliary equation-based methods [15, 16]. In particular, schemes like the modified extended direct algebraic method [17], the tanh-coth method [18], and the Jacobi elliptic function expansion technique [19] have proven successful in uncovering solitary wave structures, including exotic solitons and rogue waves. These developments are not only confined to integer-order equations but have also been extended to fractional-order NLPDEs, further modifying the flexibility of mathematical modeling in realistic physical scenarios.

Recent advancements in nonlinear wave theory have led to the development of more comprehensive models, among which the dual-mode resonant nonlinear Schrödinger equation (RNLSE) emerges as a significant extension of the classical NLSE. This generalized form explains the synchronized propagation of two interacting wave components, each governed by different dispersion and nonlinear characteristics, influenced by an embedded phase velocity parameter. Such dual-mode frameworks not only deepen our comprehending of nonlinear dispersive interactions but also serve as essential tools for modeling multi-wave phenomena in optical and plasma media. The conceptual foundation of dual-mode systems originates from the dual-mode Korteweg–de Vries (DMKdV) framework [20, 21], which demonstrates the concurrent evolution of wave trains with differential dynamical behaviors. Solitons [22, 23, 24] self-reinforcing, localized wave packets are a hallmark of nonlinear media, known for their remarkable ability to maintain shape and energy during propagation, even after mutual collisions. These structures have profound applications across optical fiber communication, plasma waves, photonic devices, and quantum systems. Specifically in inhomogeneous or nonlinear optical environments, the propagation of optical solitons is efficiently modeled by nonlinear Schrödinger-type equations that incorporate distributed nonlinearity and dispersion. The structure and interaction of such solitons are deeply influenced by the balance of nonlinearity and dispersion in the medium [25, 26].

One notable instance of dual-mode modeling is found in the second-order-in-time Korteweg–de Vries-type equation, which explains two symmetric waves co-propagating under the modulation of a phase velocity parameter λ. This DMKdV model is expressed as:

$$\Theta_{tt} - \lambda^2 \Theta_{xx} + \left(\frac{\partial}{\partial t} - \delta_1 \lambda \frac{\partial}{\partial x}\right) \Theta \Theta_x + \left(\frac{\partial}{\partial t} - \delta_2 \lambda \frac{\partial}{\partial x}\right) \Theta_{xxx} = 0, \tag{1}$$

where $\Theta = \Theta(x,t)$ denotes the wave profile, and δ_1, δ_2 are nonlinear and dispersion coefficients, respectively, satisfying $|\delta_1| \leq 1$, $|\delta_2| \leq 1$. The embedded velocity parameter λ controls the interaction strength and directionality of the coupled waves. This dual-mode model has since inspired the formulation of various higher-order and multidimensional dual-mode equations that better capture the complexity of real-world wave interactions in nonlinear systems.

The concept of dual-mode equations originates from physical systems involving the interaction of wave components in

anisotropic, layered, or inhomogeneous media. In particular, the classical DMKdV model [27] depicted the evolution of two co-propagating wave structures with distinct dispersion profiles. In the absence of interaction, the system simplifies to the conventional KdV equation. Building upon this foundation, Wazwaz and other researchers have introduced dual-mode extensions of different nonlinear evolution equations, including the KP, Burgers, modified KdV, Sharma–Tasso–Olver, and Boussinesq systems [28, 29, 30, 31, 32, 33]. These types of dual-mode equations have been demonstrated to exist in the third-order Fisher equation, the coupled-KdV equation, the coupled Burgers equation, the coupled modified KdV equation, the Kuramoto–Sivashinsky equation, the KdV-Burgers equation, and the higher order Boussinesq–Burgers system [31, 32, 33]. Through a review of the dual-mode Sharma–Tasso–Olver equation and the DMKdV equation, many new solitary wave solutions have been discovered in the literature [34, 35]. Furthermore, several scholars have extended the dual-mode notion to Schrödinger equations [36, 37]. In [38, 39], the dynamics of dual-mode events have also been thoroughly studied. It should be noted that the majority of the work mentioned above focuses on creating new dual-mode equations using Korsunsky's methodology. We anticipate that the development of fresh methods for researching dual-mode models will keep expanding.

Motivated by these advancements, the current study focuses on a generalized dual-mode RNLSE that incorporates both a Bohm-type quantum potential and a square-root Kerr nonlinearity. This formulation is particularly relevant for nonlinear optical media showing saturable refractive index behavior. The model governing the wave dynamics is expressed as [40]:

$$i(\Theta_{tt} - \lambda^2\Theta_{xx}) + \left(\frac{\partial}{\partial t} - \delta_1\lambda\frac{\partial}{\partial x}\right)\left(\mathcal{S}(|\Theta|^2)\Theta + \mu\left(\frac{|\Theta|xx}{|\Theta|}\right)\Theta\right) + \left(\frac{\partial}{\partial t} - \delta 2\lambda\frac{\partial}{\partial x}\right)\left(\frac{1}{2}\Theta_{xx}\right) = 0, \tag{2}$$

where $\mathcal{S}(|\Theta|^2)$ represents the nonlinear term governed by the square-root Kerr law, μ is the quantum correction coefficient associated with the Bohm potential, and λ denotes the phase velocity mediating the interaction between the coupled modes. This dual-mode RNLSE framework offers a robust platform for showing soliton dynamics under the combined influence of nonlinearity, dispersion, and quantum effects, allowing a deeper understanding of wave propagation in modern nonlinear optics and photonic systems.

In this work, we employ two powerful symbolic computational techniques the eMETFM and the $\left(\frac{\mathcal{G}'}{\mathcal{G}^2}\right)$-expansion method to construct exact analytical soliton solutions to Equation (2). These methods are selected for their versatility in capturing a variety of nonlinear wave structures, including bright, dark, singular, and rational solitons. Through these solutions, we analyze the dynamical role of the dispersive and nonlinear parameters, with a focus on dual-wave propagation, interaction, and structural stability. Graphical representations in the form of 2D plots, 3D profiles, and contour projections are used to visualize and interpret the structure of the derived solutions. The outcomes not only present deeper insights into the physics of nonlinear optical solitons but also open avenues for extending the dual-mode framework to other integrable and non-integrable systems.

The structure of the paper is as follows:

- **Section 2**: Describes the EMETFM and $\left(\frac{\mathcal{G}'}{\mathcal{G}^2}\right)$-expansion methods used for analytical derivations.
- **Section 3**: Presents the formulation and physical background of the dual-mode RNLSE under square-root Kerr nonlinearity and apply a traveling wave transformation.
- **Section 4**: Details the exact soliton solutions obtained through the above techniques.

- **Section 5**: Provides a physical interpretation and dynamical visualization of the results.
- **Section 6**: Concludes with key findings and outlines possible directions for future research.

2. Formulation of Methods

In this study, we explore optical soliton solutions of the dual-mode resonant nonlinear Schrödinger equation (RNLSE) governed by the square root Kerr law. To achieve this, we employ two analytical approaches: the eMETFM incorporating the Riccati equation, and the $\left(\frac{\mathcal{G}'}{\mathcal{G}^2}\right)$-expansion technique. For the purpose of this analysis, we consider a general NLPDE defined as follows:

$$\boldsymbol{\mathcal{U}}(\Theta,\ \Theta_t,\ \Theta_x,\ \Theta_{xt},\ \Theta_{xx},\ \cdots) = 0, \tag{3}$$

here, $\Theta = \Theta(x,t)$ be an unknown function of the variables x and t, involving its partial derivatives. The corresponding wave transformation is employed as follows:

$$\Theta(x,t) \quad = \quad \Lambda(\chi), \quad \text{where} \ \ \Lambda = x - \kappa t. \tag{4}$$

Here, $\Lambda(\chi)$ represents the wave amplitude, while κ is a constant associated with the wave speed. By employing a suitable sequence of transformations, Equation (3) is reduced to the following ordinary differential equation:

$$\mathscr{R}(\Lambda,\ \Lambda',\ \Lambda'',\ \cdots) = 0. \tag{5}$$

2.1. Overview of eMETEM

The eMETEM is an effective analytical technique for obtaining accurate solutions of nonlinear differential equations. Its strength lies in its ability to extract diverse soliton structures while efficiently addressing a broad class of nonlinearities, providing greater flexibility and precision compared to classical tanh-based approaches. The core principles and essential components of the eMETEM are outlined below [41]:

Step 1: Assume that the solution to Equation (5) takes the following specific form:

$$\Lambda(\chi) = \boldsymbol{\mathcal{C}}_0 + \sum_{i=0}^{m} \boldsymbol{\mathcal{C}}_i(\boldsymbol{\mathcal{T}}(\chi))^i + \sum_{i=1}^{m} \boldsymbol{\mathcal{D}}_i(\boldsymbol{\mathcal{T}}(\chi))^{-i}. \tag{6}$$

Here, $\boldsymbol{\mathcal{C}}_i$ and $\boldsymbol{\mathcal{D}}_i$ are not both zero simultaneously. When $\Lambda = \Lambda(\chi)$, the following condition holds:

$$\boldsymbol{\mathcal{T}}'(\chi) = \phi + \boldsymbol{\mathcal{T}}^2(\chi), \tag{7}$$

Here, ϕ denotes an arbitrary constant.

Step 2: To determine the value of m, the balancing principle is applied to Equation (5).

Step 3: Equations (6) and (7) are substituted into Equation (5), and the resulting expression is organized by powers of $\boldsymbol{\mathcal{T}}(\chi)$. The coefficients of each distinct power are then set to zero, leading to an overdetermined system of nonlinear algebraic equations. Solving this system yields the values of the unknown parameters $\boldsymbol{\mathcal{C}}_i$ and $\boldsymbol{\mathcal{D}}_i$, which are subsequently used to construct the exact solution of Equation (3).

Theorem 1. *If $\phi < 0$, then the solutions of Equation (7) are expressed in hyperbolic form [42].*

Proof. *Given that $\phi < 0$, the Riccati equation admits hyperbolic-type solutions of the following form, where $\epsilon = \pm 1$:*

$$\begin{cases} \boldsymbol{\mathcal{T}}_1(\chi) = \sqrt{-\phi}\tanh\left(\sqrt{-\phi}\,(\chi+\chi_0)\right). \\ \boldsymbol{\mathcal{T}}_2(\chi) = -\sqrt{-\phi}\coth\left(\sqrt{-\phi}\,(\chi+\chi_0)\right). \\ \boldsymbol{\mathcal{T}}_3(\chi) = -\sqrt{-\phi}\left(\tanh\left(2\sqrt{-\phi}\,(\chi+\chi_0)\right) + i\epsilon sech\left(2\sqrt{-\phi}\,(\chi+\chi_0)\right)\right). \\ \boldsymbol{\mathcal{T}}_4(\chi) = \frac{\phi-\sqrt{-\phi}\tanh\left(\sqrt{-\phi}(\chi+\chi_0)\right)}{\sqrt{-\phi}\tanh\left(\sqrt{-\phi}(\chi+\chi_0)\right)+1}. \\ \boldsymbol{\mathcal{T}}_5(\chi) = \frac{\sqrt{-\phi}\left(5-4\cosh\left(2\sqrt{-\phi}(\chi+\chi_0)\right)\right)}{4\sinh\left(2\sqrt{-\phi}(\chi+\chi_0)\right)+3}. \\ \boldsymbol{\mathcal{T}}_6(\chi) = \frac{\epsilon\sqrt{\left(k_1^2+k_2^2\right)(-\phi)}-k_1\sqrt{-\phi}\cosh\left(2\sqrt{-\phi}(\chi+\chi_0)\right)}{k_1\sinh\left(2\sqrt{-\phi}(\chi+\chi_0)\right)+k_2}. \\ \boldsymbol{\mathcal{T}}_7(\chi) = \sqrt{-\phi}\epsilon\left(1-\frac{2k_1}{k_1+\cosh\left(2\sqrt{-\phi}(\chi+\chi_0)\right)-\epsilon\sinh\left(2\sqrt{-\phi}(\chi+\chi_0)\right)}\right). \end{cases} \tag{8}$$

In this instance, k_1 and k_2 are two constants with real values.

Theorem 2. *If $\phi > 0$, then the solutions of Equation (7) are of trigonometric type [42].*

Proof. *For $\phi > 0$, the Riccati equation yields trigonometric solutions of the following form, where $\epsilon = \pm 1$:*

$$\begin{cases} \boldsymbol{\mathcal{T}}_8(\chi) = \sqrt{\phi}\tan\left(\sqrt{\phi}\,(\chi+\chi_0)\right). \\ \boldsymbol{\mathcal{T}}_9(\chi) = \sqrt{\phi}\cot\left(\sqrt{\phi}\,(\chi+\chi_0)\right). \\ \boldsymbol{\mathcal{T}}_{10}(\chi) = \sqrt{\phi}\left(\tan\left(2\sqrt{\phi}\,(\chi+\chi_0)\right) + \epsilon\sec\left(2\sqrt{\phi}\,(\chi+\chi_0)\right)\right). \\ \boldsymbol{\mathcal{T}}_{11}(\chi) = -\frac{\sqrt{\phi}\left(1-\tan\left(\sqrt{\phi}(\chi+\chi_0)\right)\right)}{\tan\left(\sqrt{\phi}(\chi+\chi_0)\right)+1}. \\ \boldsymbol{\mathcal{T}}_{12}(\chi) = \frac{\sqrt{\phi}\left(4-5\cos\left(2\sqrt{\phi}(\chi+\chi_0)\right)\right)}{5\sin\left(2\sqrt{\phi}(\chi+\chi_0)\right)+3}. \\ \boldsymbol{\mathcal{T}}_{13}(\chi) = \frac{\epsilon\sqrt{\left(k_1^2-k_2^2\right)\phi}-k_1\sqrt{\phi}\cos\left(2\sqrt{\phi}(\chi+\chi_0)\right)}{k_1\sin\left(2\sqrt{\phi}(\chi+\chi_0)\right)+k_2}. \\ \boldsymbol{\mathcal{T}}_{14}(\chi) = i\sqrt{\phi}\epsilon\left(1-\frac{2k_1}{k_1+\cos\left(2\sqrt{\phi}(\chi+\chi_0)\right)-i\epsilon\sin\left(2\sqrt{\phi}(\chi+\chi_0)\right)}\right). \end{cases} \tag{9}$$

Here, k_1 and k_2 denote two constants belonging to the set of real numbers.

Theorem 3. *If $\phi = 0$, then Equation (7) admits a rational solution [42].*

Proof. *When $\phi = 0$, the Riccati equation yields the following rational-form solution, where $\epsilon = \pm 1$:*

$$\left\{\boldsymbol{\mathcal{T}}_{15}(\chi) = -\frac{1}{\chi+\chi_0}. \right. \tag{10}$$

2.2. Overview of $\left(\frac{\mathcal{G}'}{\mathcal{G}^2}\right)$-expansion function method

The $\left(\frac{\boldsymbol{\mathcal{G}'}}{\boldsymbol{\mathcal{G}^2}}\right)$-expansion method is a powerful analytical technique for obtaining exact solutions of NPDEs. The method has been successfully applied to a wide range of nonlinear models in mathematical physics, yielding exact solutions expressed in terms of trigonometric, hyperbolic, and rational functions.

The fundamental steps of the $\left(\frac{\mathcal{G}'}{\mathcal{G}^2}\right)$-expansion method are described below [43]:
As a first step, we seek an exact solution of Equation (16) in the following form:

$$\Lambda(\chi) = \mathcal{K}_0 + \sum_{i=0}^{m} \mathcal{K}_i \left(\frac{\mathcal{G}'}{\mathcal{G}^2}\right)^i + \sum_{i=1}^{m} \mathcal{R}_i \left(\frac{\mathcal{G}'}{\mathcal{G}^2}\right)^{-i}, \tag{11}$$

where $\mathcal{K}_i$ and $\mathcal{R}_i$ are not simultaneously equal to zero. For instance, let $\Gamma = \Gamma(\chi)$, and assume that the corresponding solution of the associated ODE is given by $\mathcal{G} = \mathcal{G}(\chi)$.

$$\left(\frac{\mathcal{G}'}{\mathcal{G}^2}\right)' = \Pi + \varrho \left(\frac{\mathcal{G}'}{\mathcal{G}^2}\right)^2, \tag{12}$$

where Π and ϱ are constants. As a result, the $\left(\frac{\mathcal{G}'}{\mathcal{G}^2}\right)$-expansion method yields three distinct types of solutions. Accordingly, the outcome of Equation (12) can be expressed as follows:

Theorem 4. *If $\Pi\varrho > 0$, then Equation (12) admits trigonometric-type solutions [43].*

Proof. *Given that $\Pi\varrho > 0$, the corresponding algebraic equation yields solutions of trigonometric form as follows:*

$$\left(\frac{\mathcal{G}'}{\mathcal{G}^2}\right) = \sqrt{\frac{\Pi}{\varrho}} \left(\frac{c_2 \sin\left(\chi\sqrt{\Pi\varrho}\right) + c_1 \cos\left(\chi\sqrt{\Pi\varrho}\right)}{c_2 \cos\left(\chi\sqrt{\Pi\varrho}\right) - c_1 \sin\left(\chi\sqrt{\Pi\varrho}\right)}\right). \tag{13}$$

Theorem 5. *If $\Pi\varrho < 0$, then Equation (12) admits hyperbolic-type solutions [43].*

Proof. *Since $\Pi\varrho < 0$, the relating algebraic equation leads to solutions of hyperbolic form, as shown below:*

$$\left(\frac{\mathcal{G}'}{\mathcal{G}^2}\right) = -\sqrt{\frac{\Pi\varrho}{\varrho}} \left(\frac{c_1 \sinh\left(2\chi\sqrt{\Pi\varrho}\right) + c_1 \cosh\left(2\chi\sqrt{\Pi\varrho}\right) + c_2}{c_1 \sinh\left(2\chi\sqrt{\Pi\varrho}\right) + c_1 \cosh\left(2\chi\sqrt{\Pi\varrho}\right) - c_2}\right). \tag{14}$$

Theorem 6. *If $\Pi \neq 0$ and $\varrho = 0$, then Equation (12) yields rational-type solutions [43].*

Proof. *Under the conditions $\Pi \neq 0$ and $\varrho = 0$, the corresponding algebraic equation produces solutions of rational form, as given below:*

$$\left(\frac{\mathcal{G}'}{\mathcal{G}^2}\right) = \left(-\frac{c_1}{\varrho\left(c_1\chi + c_2\right)}\right). \tag{15}$$

In this context, c_1 and c_2 are arbitrary constants. The resulting system of algebraic equations is obtained by substituting the expressions from Equations (11) and (12) into Equation (5), collecting like terms based on the powers of $\left(\frac{\mathcal{G}'}{\mathcal{G}^2}\right)$, and equating the corresponding coefficients to zero. This system is then solved using the Mathematica software.

3. Mathematical Analysis

The square root Kerr law describes a nonlinear interaction in which a system's output depends on a parameter Θ such as intensity, energy, or field amplitude through a mathematical expression of the form $S(\Theta) = \sqrt{\Theta}$. This representation results in a gradual and smooth nonlinear structure. Unlike to the traditional Kerr effect, which assumes a direct (linear) proportionality with Θ, this model accounts for situations where the nonlinear response grows at a

slower rate. Such structure is characteristic of systems exhibiting saturable nonlinearities, commonly found in certain optical environments.

Substituting $S(\Theta) = \sqrt{\Theta}$ [37] in Equation (2), we derive:

$$i(\Theta_{tt} - \lambda^2\Theta_{xx}) + \left(\frac{\partial}{\partial t} - \delta_1\lambda\frac{\partial}{\partial x}\right)\left(|\Theta|\Theta + \mu\left(\frac{|\Theta|_{xx}}{|\Theta|}\right)\Theta\right) + \left(\frac{\partial}{\partial t} - \delta_2\lambda\frac{\partial}{\partial x}\right)\left(\frac{1}{2}\Theta_{xx}\right) = 0. \tag{16}$$

In order to solve Equation (16), the wave functions Θ are defined as follows:

$$\Theta(x,t) = \Lambda(\chi)e^{i(\Psi)},\ \chi = x - \kappa t,\ \Psi = \alpha(x + \gamma t). \tag{17}$$

After splitting into imaginary and real portions, we determine a system of non-linear ODEs by putting Equation (17) into Equation (16). This gives us the following:

$$\begin{cases} Im:\ (-2\gamma^2 + 2\lambda^2 + \alpha\sigma_2\lambda - \alpha\gamma)\alpha^2\Lambda + 2\alpha(\gamma - \sigma_1\lambda)\Lambda^2 + \\ (2\kappa^2 - 2\lambda^2 + \alpha\gamma - 2\alpha\kappa - 3\sigma_2\lambda\alpha - 2\mu\alpha(\sigma_1\lambda - \gamma))\Lambda^{''} = 0. \end{cases} \tag{18}$$

$$\begin{cases} Re:\ \alpha(4\gamma\kappa + 4\lambda^2 + 3\sigma_2\lambda\alpha - 2\alpha\gamma + \alpha\kappa)\Lambda - 2(\sigma_1\lambda + \kappa)\Lambda^2 - \\ (\kappa + \sigma_2\lambda + 2\mu(\kappa + \alpha\lambda))\Lambda^{''} = 0. \end{cases} \tag{19}$$

By balancing the dominant nonlinear term Λ in Equation (19) with the highest-order derivative term $\Lambda^{''}$, we determine that $m = 2$.

4. Implementation of eMETFM

We investigate the soliton solutions of Equation (16) using the eMETFM. Since the transformation of Equation (16) into an ordinary differential equation has already been addressed in Sect. 4, we now focus on Equation (19). Referring to Equation (6) and adopting this value of m, the general solution to Equation (19) is given by:

$$\Lambda(\chi) = \boldsymbol{\mathcal{C}}_0 + \boldsymbol{\mathcal{C}}_1\boldsymbol{\mathcal{T}}(\chi) + \boldsymbol{\mathcal{C}}_2\boldsymbol{\mathcal{T}}(\chi)^2 + \frac{\boldsymbol{\mathcal{D}}_1}{\boldsymbol{\mathcal{T}}(\chi)} + \frac{\boldsymbol{\mathcal{D}}_2}{\boldsymbol{\mathcal{T}}(\chi)^2}. \tag{20}$$

Substituting Equation (20) into Equation (19) via the relation in Equation (7), we obtain a polynomial in powers of $\boldsymbol{\mathcal{T}}(\chi)$. By grouping terms according to identical exponents of $\boldsymbol{\mathcal{T}}^i(\chi)$, for $i = 0, \pm1, \pm2, \pm3$, and equating the coefficients

of each term to zero, we derive a corresponding algebraic system.

$$\begin{cases}
\boldsymbol{\mathcal{T}}(\chi)^{-4}: & -12\delta_1\lambda\mu\boldsymbol{\mathcal{D}}_2\phi^2-6\delta_2\lambda\boldsymbol{\mathcal{D}}_2\phi^2-2\delta_1\lambda\boldsymbol{\mathcal{D}}_2^2-12\kappa\mu\boldsymbol{\mathcal{D}}_2\phi^2-6\kappa\boldsymbol{\mathcal{D}}_2\phi^2-2\kappa\boldsymbol{\mathcal{D}}_2^2=0,\\
\boldsymbol{\mathcal{T}}(\chi)^{-3}: & -4\delta_1\lambda\mu\boldsymbol{\mathcal{D}}_1\phi^2-2\delta_2\lambda\boldsymbol{\mathcal{D}}_1\phi^2-4\delta_1\lambda\boldsymbol{\mathcal{D}}_1\boldsymbol{\mathcal{D}}_2-4\kappa\mu\boldsymbol{\mathcal{D}}_1\phi^2-2\kappa\boldsymbol{\mathcal{D}}_1\phi^2-4\kappa\boldsymbol{\mathcal{D}}_1\boldsymbol{\mathcal{D}}_2=0,\\
\boldsymbol{\mathcal{T}}(\chi)^{-2}: & -4\boldsymbol{\mathcal{C}}_0\delta_1\lambda\boldsymbol{\mathcal{D}}_2-4\boldsymbol{\mathcal{C}}_0\kappa\boldsymbol{\mathcal{D}}_2-2\alpha^2\gamma\boldsymbol{\mathcal{D}}_2+3\alpha^2\delta_2\lambda\boldsymbol{\mathcal{D}}_2+\alpha^2\kappa\boldsymbol{\mathcal{D}}_2+4\alpha\gamma\kappa\boldsymbol{\mathcal{D}}_2+4\alpha\lambda^2\boldsymbol{\mathcal{D}}_2-\\
& 16\delta_1\lambda\mu\boldsymbol{\mathcal{D}}_2\phi-8\delta_2\lambda\boldsymbol{\mathcal{D}}_2\phi-2\delta_1\lambda\boldsymbol{\mathcal{D}}_1^2-16\kappa\mu\boldsymbol{\mathcal{D}}_2\phi-8\kappa\boldsymbol{\mathcal{D}}_2\phi-2\kappa\boldsymbol{\mathcal{D}}_1^2=0,\\
\boldsymbol{\mathcal{T}}(\chi)^{-1}: & -4\boldsymbol{\mathcal{C}}_0\delta_1\lambda\boldsymbol{\mathcal{D}}_1-4\boldsymbol{\mathcal{C}}_1\delta_1\lambda\boldsymbol{\mathcal{D}}_2-4\boldsymbol{\mathcal{C}}_0\kappa\boldsymbol{\mathcal{D}}_1-4\boldsymbol{\mathcal{C}}_1\kappa\boldsymbol{\mathcal{D}}_2-2\alpha^2\gamma\boldsymbol{\mathcal{D}}_1+3\alpha^2\delta_2\lambda\boldsymbol{\mathcal{D}}_1+\alpha^2\kappa\boldsymbol{\mathcal{D}}_1+\\
& 4\alpha\gamma\kappa\boldsymbol{\mathcal{D}}_1+4\alpha\lambda^2\boldsymbol{\mathcal{D}}_1-4\delta_1\lambda\mu\boldsymbol{\mathcal{D}}_1\phi-2\delta_2\lambda\boldsymbol{\mathcal{D}}_1\phi-4\kappa\mu\boldsymbol{\mathcal{D}}_1\phi-2\kappa\boldsymbol{\mathcal{D}}_1\phi=0,\\
\boldsymbol{\mathcal{T}}(\chi)^{0}: & -2\alpha^2\gamma\boldsymbol{\mathcal{C}}_0+3\alpha^2\boldsymbol{\mathcal{C}}_0\delta_2\lambda+\alpha^2\boldsymbol{\mathcal{C}}_0\kappa+4\alpha\gamma\boldsymbol{\mathcal{C}}_0\kappa+4\alpha\boldsymbol{\mathcal{C}}_0\lambda^2-4\boldsymbol{\mathcal{C}}_2\delta_1\lambda\mu\phi^2-2\boldsymbol{\mathcal{C}}_2\delta_2\lambda\phi^2-\\
& 2\boldsymbol{\mathcal{C}}_0^2\delta_1\lambda-4\boldsymbol{\mathcal{C}}_2\kappa\mu\phi^2-2\boldsymbol{\mathcal{C}}_2\kappa\phi^2-2\boldsymbol{\mathcal{C}}_0^2\kappa-4\boldsymbol{\mathcal{C}}_1\delta_1\lambda\boldsymbol{\mathcal{D}}_1-4\boldsymbol{\mathcal{C}}_2\delta_1\lambda\boldsymbol{\mathcal{D}}_2-4\boldsymbol{\mathcal{C}}_1\kappa\boldsymbol{\mathcal{D}}_1-4\boldsymbol{\mathcal{C}}_2\kappa\boldsymbol{\mathcal{D}}_2-\\
& 4\delta_1\lambda\mu\boldsymbol{\mathcal{D}}_2-2\delta_2\lambda\boldsymbol{\mathcal{D}}_2-4\kappa\mu\boldsymbol{\mathcal{D}}_2-2\kappa\boldsymbol{\mathcal{D}}_2=0,\\
\boldsymbol{\mathcal{T}}(\chi)^{4}: & -12\boldsymbol{\mathcal{C}}_2\delta_1\lambda\mu-2\boldsymbol{\mathcal{C}}_2^2\delta_1\lambda-6\boldsymbol{\mathcal{C}}_2\delta_2\lambda-12\boldsymbol{\mathcal{C}}_2\kappa\mu-2\boldsymbol{\mathcal{C}}_2^2\kappa-6\boldsymbol{\mathcal{C}}_2\kappa=0,\\
\boldsymbol{\mathcal{T}}(\chi)^{3}: & -4\boldsymbol{\mathcal{C}}_1\delta_1\lambda\mu-4\boldsymbol{\mathcal{C}}_2\boldsymbol{\mathcal{C}}_1\delta_1\lambda-2\boldsymbol{\mathcal{C}}_1\delta_2\lambda-4\boldsymbol{\mathcal{C}}_1\kappa\mu-2\boldsymbol{\mathcal{C}}_1\kappa-4\boldsymbol{\mathcal{C}}_2\boldsymbol{\mathcal{C}}_1\kappa=0,\\
\boldsymbol{\mathcal{T}}(\chi)^{2}: & -2\alpha^2\gamma\boldsymbol{\mathcal{C}}_2+3\alpha^2\boldsymbol{\mathcal{C}}_2\delta_2\lambda+\alpha^2\boldsymbol{\mathcal{C}}_2\kappa+4\alpha\gamma\boldsymbol{\mathcal{C}}_2\kappa+4\alpha\boldsymbol{\mathcal{C}}_2\lambda^2-16\boldsymbol{\mathcal{C}}_2\delta_1\lambda\mu\phi-\\
& 8\boldsymbol{\mathcal{C}}_2\delta_2\lambda\phi-2\boldsymbol{\mathcal{C}}_1^2\delta_1\lambda-4\boldsymbol{\mathcal{C}}_0\boldsymbol{\mathcal{C}}_2\delta_1\lambda-16\boldsymbol{\mathcal{C}}_2\kappa\mu\phi-8c_2\kappa\phi-2\boldsymbol{\mathcal{C}}_1^2\kappa-4\boldsymbol{\mathcal{C}}_0\boldsymbol{\mathcal{C}}_2\kappa=0,\\
\boldsymbol{\mathcal{T}}(\chi)^{1}: & -2\alpha^2\gamma\boldsymbol{\mathcal{C}}_1+3\alpha^2\boldsymbol{\mathcal{C}}_1\delta_2\lambda+\alpha^2\boldsymbol{\mathcal{C}}_1\kappa+4\alpha\gamma\boldsymbol{\mathcal{C}}_1\kappa+4\alpha\boldsymbol{\mathcal{C}}_1\lambda^2-4\boldsymbol{\mathcal{C}}_1\delta_1\lambda\mu\phi-\\
& 2\boldsymbol{\mathcal{C}}_1\delta_2\lambda\phi-4\boldsymbol{\mathcal{C}}_0\boldsymbol{\mathcal{C}}_1\delta_1\lambda-4\boldsymbol{\mathcal{C}}_1\kappa\mu\phi-2\boldsymbol{\mathcal{C}}_1\kappa\phi-4\boldsymbol{\mathcal{C}}_0\boldsymbol{\mathcal{C}}_1\kappa-4\boldsymbol{\mathcal{C}}_2\delta_1\lambda\boldsymbol{\mathcal{D}}_1-4\boldsymbol{\mathcal{C}}_2\kappa\boldsymbol{\mathcal{D}}_1=0.
\end{cases}\tag{21}$$

The corresponding families of soliton solutions can be derived.

$$\begin{cases}
\boldsymbol{\mathcal{C}}_0=-\frac{3\phi(2\delta_1\lambda\mu+\delta_2\lambda+2\kappa\mu+\kappa)}{\delta_1\lambda+\kappa},\ \boldsymbol{\mathcal{C}}_1=0,\ \boldsymbol{\mathcal{C}}_2=-\frac{3(2\delta_1\lambda\mu+\delta_2\lambda+2\kappa\mu+\kappa)}{\delta_1\lambda+\kappa},\ \boldsymbol{\mathcal{D}}_1=0,\ \boldsymbol{\mathcal{D}}_2=0,\\
\gamma=\frac{3\alpha^2\delta_2\lambda+\alpha^2\kappa+4\alpha\lambda^2+8\delta_1\lambda\mu\phi+4\delta_2\lambda\phi+8\kappa\mu\phi+4\kappa\phi}{2\alpha^2-4\alpha\kappa}.
\end{cases}\tag{22}$$

The new solitary wave solutions of Equation (19) are therefore given by:

- **Hyperbolic solutions:**

$$\Theta_1(x,t)=\left[\frac{3\phi\tanh^2\left((\chi+\pi_0)\sqrt{-\phi}\right)(2\delta_1\lambda\mu+\delta_2\lambda+2\kappa\mu+\kappa)}{\delta_1\lambda+\kappa}-\frac{3\phi\,(2\delta_1\lambda\mu+\delta_2\lambda+2\kappa\mu+\kappa)}{\delta_1\lambda+\kappa}\right]\times e^{i\alpha(x+\gamma t)}.\tag{23}$$

$$\Theta_2(x,t)=\left[\frac{3\phi\coth^2\left((\chi+\pi_0)\sqrt{-\phi}\right)(2\delta_1\lambda\mu+\delta_2\lambda+2\kappa\mu+\kappa)}{\delta_1\lambda+\kappa}-\frac{3\phi\,(2\delta_1\lambda\mu+\delta_2\lambda+2\kappa\mu+\kappa)}{\delta_1\lambda+\kappa}\right]\times e^{i\alpha(x+\gamma t)}.\tag{24}$$

$$\Theta_3(x,t)=\left[\frac{3\phi\,(2\delta_1\lambda\mu+\delta_2\lambda+2\kappa\mu+\kappa)\left(\tanh\left(2\,(\chi+\chi_0)\sqrt{-\phi}\right)+i\epsilon\,\mathrm{sech}\left(2\,(\chi+\chi_0)\sqrt{-\phi}\right)\right)^2}{\delta_1\lambda+\kappa}-\frac{3\phi\,(2\delta_1\lambda\mu+\delta_2\lambda+2\kappa\mu+\kappa)}{\delta_1\lambda+\kappa}\right]\times e^{i\alpha(x+\gamma t)}.\tag{25}$$

$$\Theta_4(x,t)=\left[-\frac{3\left(\phi-\sqrt{-\phi}\tanh\left((\chi+\chi_0)\sqrt{-\phi}\right)\right)^2(2\delta_1\lambda\mu+\delta_2\lambda+2\kappa\mu+\kappa)}{(\delta_1\lambda+\kappa)\left(\sqrt{-\phi}\tanh\left((\chi+\chi_0)\sqrt{-\phi}\right)+1\right)^2}-\frac{3\phi\,(2\delta_1\lambda\mu+\delta_2\lambda+2\kappa\mu+\kappa)}{\delta_1\lambda+\kappa}\right]\times e^{i\alpha(x+\gamma t)}.\tag{26}$$

$$\Theta_5(x,t)=\left[\frac{3\phi\left(5-4\cosh\left(2\,(\chi+\chi_0)\sqrt{-\phi}\right)\right)^2(2\delta_1\lambda\mu+\delta_2\lambda+2\kappa\mu+\kappa)}{(\delta_1\lambda+\kappa)\left(4\sinh\left(2\,(\chi+\chi_0)\sqrt{-\phi}\right)+3\right)^2}-\frac{3\phi\,(2\delta_1\lambda\mu+\delta_2\lambda+2\kappa\mu+\kappa)}{\delta_1\lambda+\kappa}\right]\times e^{i\alpha(x+\gamma t)}.\tag{27}$$

$$\Theta_6(x,t)=\left[-\frac{3\left(2\delta_1\lambda\mu+\delta_2\lambda+2\kappa\mu+\kappa\right)\left(\epsilon\sqrt{\left(f_1^2+f_2^2\right)\left(-\phi\right)}-f_1\sqrt{-\phi}\cosh\left(2\left(\chi+\chi_0\right)\sqrt{-\phi}\right)\right)^2}{\left(\delta_1\lambda+\kappa\right)\left(f_1\sinh\left(2\left(\chi+\chi_0\right)\sqrt{-\phi}\right)+f_2\right)^2}-\frac{3\phi\left(2\delta_1\lambda\mu+\delta_2\lambda+2\kappa\mu+\kappa\right)}{\delta_1\lambda+\kappa}\right]\times e^{i\alpha(x+\gamma t)}. \quad (28)$$

$$\Theta_7(x,t)=\left[\frac{3\epsilon^2\phi\left(2\delta_1\lambda\mu+\delta_2\lambda+2\kappa\mu+\kappa\right)\left(1-\frac{2f_1}{f_1-\epsilon\sinh\left(2(\chi+\chi_0)\sqrt{-\phi}\right)+\cosh\left(2(\chi+\chi_0)\sqrt{-\phi}\right)}\right)^2}{\delta_1\lambda+\kappa}-\frac{3\phi\left(2\delta_1\lambda\mu+\delta_2\lambda+2\kappa\mu+\kappa\right)}{\delta_1\lambda+\kappa}\right]\times e^{i\alpha(x+\gamma t)}. \quad (29)$$

- **Trigonometric solution:**

$$\Theta_8(x,t)=\left[-\frac{3\phi\tan^2\left(\left(\chi+\chi_0\right)\sqrt{\phi}\right)\left(2\delta_1\lambda\mu+\delta_2\lambda+2\kappa\mu+\kappa\right)}{\delta_1\lambda+\kappa}-\frac{3\phi\left(2\delta_1\lambda\mu+\delta_2\lambda+2\kappa\mu+\kappa\right)}{\delta_1\lambda+\kappa}\right]\times e^{i\alpha(x+\gamma t)}. \quad (30)$$

$$\Theta_9(x,t)=\left[-\frac{3\phi\cot^2\left(\left(\chi+\chi_0\right)\sqrt{\phi}\right)\left(2\delta_1\lambda\mu+\delta_2\lambda+2\kappa\mu+\kappa\right)}{\delta_1\lambda+\kappa}-\frac{3\phi\left(2\delta_1\lambda\mu+\delta_2\lambda+2\kappa\mu+\kappa\right)}{\delta_1\lambda+\kappa}\right]\times e^{i\alpha(x+\gamma t)}. \quad (31)$$

$$\Theta_{10}(x,t)=\left[-\frac{3\phi\left(2\delta_1\lambda\mu+\delta_2\lambda+2\kappa\mu+\kappa\right)\left(\epsilon\sec\left(2\left(\chi+\chi_0\right)\sqrt{\phi}\right)+\tan\left(2\left(\chi+\chi_0\right)\sqrt{\phi}\right)\right)^2}{\delta_1\lambda+\kappa}\right]\times e^{i\alpha(x+\gamma t)}. \quad (32)$$

$$\Theta_{11}(x,t)=\left[-\frac{3\phi\left(1-\tan\left(\left(\chi+\chi_0\right)\sqrt{\phi}\right)\right)^2\left(2\delta_1\lambda\mu+\delta_2\lambda+2\kappa\mu+\kappa\right)}{\left(\delta_1\lambda+\kappa\right)\left(\tan\left(\left(\chi+\chi_0\right)\sqrt{\phi}\right)+1\right)^2}-\frac{3\phi\left(2\delta_1\lambda\mu+\delta_2\lambda+2\kappa\mu+\kappa\right)}{\delta_1\lambda+\kappa}\right]\times e^{i\alpha(x+\gamma t)}. \quad (33)$$

$$\Theta_{12}(x,t)=\left[-\frac{3\phi\left(4-5\cos\left(2\left(\chi+\chi_0\right)\sqrt{\phi}\right)\right)^2\left(2\delta_1\lambda\mu+\delta_2\lambda+2\kappa\mu+\kappa\right)}{\left(\delta_1\lambda+\kappa\right)\left(5\sin\left(2\left(\chi+\chi_0\right)\sqrt{\phi}\right)+3\right)^2}-\frac{3\phi\left(2\delta_1\lambda\mu+\delta_2\lambda+2\kappa\mu+\kappa\right)}{\delta_1\lambda+\kappa}\right]\times e^{i\alpha(x+\gamma t)}. \quad (34)$$

$$\Theta_{13}(x,t)=\left[-\frac{3\left(2\delta_1\lambda\mu+\delta_2\lambda+2\kappa\mu+\kappa\right)\left(\epsilon\sqrt{\left(f_1^2-f_2^2\right)\phi}-f_1\sqrt{\phi}\cos\left(2\left(\chi+\chi_0\right)\sqrt{\phi}\right)\right)^2}{\left(\delta_1\lambda+\kappa\right)\left(f_1\sin\left(2\left(\chi+\chi_0\right)\sqrt{\phi}\right)+f_2\right)^2}-\frac{3\phi\left(2\delta_1\lambda\mu+\delta_2\lambda+2\kappa\mu+\kappa\right)}{\delta_1\lambda+\kappa}\right]\times e^{i\alpha(x+\gamma t)}. \quad (35)$$

$$\Theta_{14}(x,t)=\left[\frac{3\epsilon^2\phi\left(2\delta_1\lambda\mu+\delta_2\lambda+2\kappa\mu+\kappa\right)\left(1-\frac{2f_1}{f_1-i\epsilon\sin\left(2(\chi+\chi_0)\sqrt{\phi}\right)+\cos\left(2(\chi+\chi_0)\sqrt{\phi}\right)}\right)^2}{\delta_1\lambda+\kappa}-\frac{3\phi\left(2\delta_1\lambda\mu+\delta_2\lambda+2\kappa\mu+\kappa\right)}{\delta_1\lambda+\kappa}\right]\times e^{i\alpha(x+\gamma t)}. \quad (36)$$

- **Rational solution:**

$$\Theta_{15}(x,t)=\left[-\frac{3\left(2\delta_1\lambda\mu+\delta_2\lambda+2\kappa\mu+\kappa\right)}{\left(\chi+\chi_0\right)^2\left(\delta_1\lambda+\kappa\right)}-\frac{3\phi\left(2\delta_1\lambda\mu+\delta_2\lambda+2\kappa\mu+\kappa\right)}{\delta_1\lambda+\kappa}\right]\times e^{i\alpha(x+\gamma t)}. \quad (37)$$

For all above solutions $\chi=x-\kappa t$ and $\gamma=\frac{3\alpha^2\delta_2\lambda+\alpha^2\kappa+4\alpha\lambda^2+8\delta_1\lambda\mu\phi+4\delta_2\lambda\phi+8\kappa\mu\phi+4\kappa\phi}{2\alpha^2-4\alpha\kappa}$.

Remark 1.

In many earlier studies utilizing the eMETFM, the parameter ϕ appearing in the Riccati auxiliary equation is commonly assumed to be a fixed constant. In the present work, however, ϕ is treated as an adjustable parameter. This modification is necessary because the algebraic system derived from Equation (19) may produce only trivial or degenerate solutions when ϕ is restricted to a predetermined constant value. By allowing ϕ to remain flexible during the solution process, the Riccati equation generates multiple families of auxiliary functions, which in turn lead to a broader class of analytical wave structures. In particular, the sign of ϕ directly determines the type of solutions obtained: hyperbolic solutions when $\phi<0$, trigonometric solutions when $\phi>0$, and rational solutions when $\phi=0$, as described in Theorems 1–3. Therefore, treating ϕ as an undetermined parameter increases the adaptability of the method and facilitates the construction of richer soliton structures for the considered nonlinear system.

4.1. Application of the $(\frac{\mathcal{G}'}{\mathcal{G}})$-expansion function method

According to the $\left(\frac{\mathcal{G}'}{\mathcal{G}}\right)$-expansion method, the solution of Equation (19) is considered in the form:

$$\Lambda(\chi) = \mathcal{K}_0 + \mathcal{K}_1\left(\frac{\mathcal{G}'}{\mathcal{G}}\right) + \mathcal{K}_2\left(\frac{\mathcal{G}'}{\mathcal{G}}\right)^2 + \mathcal{R}_1\left(\frac{\mathcal{G}'}{\mathcal{G}}\right)^{-1} + \mathcal{R}_2\left(\frac{\mathcal{G}'}{\mathcal{G}}\right)^{-2}, \tag{38}$$

where $\mathcal{G} = \mathcal{G}(\chi)$ is the solution of the ODE Equation (12). By including Equation (38) and Equation (12) into Equation (19), we formulate a system of mathematical equations, which is presented as:

$$\begin{cases}
\left(\frac{\mathcal{G}'}{\mathcal{G}^2}\right)^{-4}: & -12\delta_1\lambda\mu\Pi^2\mathcal{R}_2 - 6\delta_2\lambda\Pi^2\mathcal{R}_2 - 2\delta_1\lambda\mathcal{R}_2^2 - 12\kappa\mu\Pi^2\mathcal{R}_2 - 6\kappa\Pi^2\mathcal{R}_2 - 2\kappa\mathcal{R}_2^2 = 0,\\
\left(\frac{\mathcal{G}'}{\mathcal{G}^2}\right)^{-3}: & -4\delta_1\lambda\mu\Pi^2\mathcal{R}_1 - 2\delta_2\lambda\Pi^2\mathcal{R}_1 - 4\delta_1\lambda\mathcal{R}_1\mathcal{R}_2 - 4\kappa\mu\Pi^2\mathcal{R}_1 - 2\kappa\Pi^2\mathcal{R}_1 - 4\kappa\mathcal{R}_1\mathcal{R}_2 = 0,\\
\left(\frac{\mathcal{G}'}{\mathcal{G}^2}\right)^{-2}: & -4\delta_1\lambda\mathcal{K}_0\mathcal{R}_2 - 4\kappa\mathcal{K}_0\mathcal{R}_2 - 2\alpha^2\gamma\mathcal{R}_2 + 3\alpha^2\delta_2\lambda\mathcal{R}_2 + \alpha^2\kappa\mathcal{R}_2 + 4\alpha\gamma\kappa\mathcal{R}_2 + 4\alpha\lambda^2\mathcal{R}_2 -\\
& 16\delta_1\lambda\mu\Pi\mathcal{R}_2\varrho - 8\delta_2\lambda\Pi\mathcal{R}_2\varrho - 2\delta_1\lambda\mathcal{R}_1^2 - 16\kappa\mu\Pi\mathcal{R}_2\varrho - 8\kappa\Pi\mathcal{R}_2\varrho - 2\kappa\mathcal{R}_1^2 = 0,\\
\left(\frac{\mathcal{G}'}{\mathcal{G}^2}\right)^{-1}: & -4\delta_1\lambda\mathcal{K}_0\mathcal{R}_1 - 4\delta_1\lambda\mathcal{K}_1\mathcal{R}_2 - 4\kappa\mathcal{K}_0\mathcal{R}_1 - 4\kappa\mathcal{K}_1\mathcal{R}_2 - 2\alpha^2\gamma\mathcal{R}_1 + 3\alpha^2\delta_2\lambda\mathcal{R}_1 + \alpha^2\kappa\mathcal{R}_1 +\\
& 4\alpha\gamma\kappa\mathcal{R}_1 + 4\alpha\lambda^2\mathcal{R}_1 - 4\delta_1\lambda\mu\Pi\mathcal{R}_1\varrho - 2\delta_2\lambda\Pi\mathcal{R}_1\varrho - 4\kappa\mu\Pi\mathcal{R}_1\varrho - 2\kappa\Pi\mathcal{R}_1\varrho = 0,\\
\left(\frac{\mathcal{G}'}{\mathcal{G}^2}\right)^{0}: & -2\alpha^2\gamma\mathcal{K}_0 + 3\alpha^2\delta_2\lambda\mathcal{K}_0 + \alpha^2\kappa\mathcal{K}_0 + 4\alpha\gamma\kappa\mathcal{K}_0 + 4\alpha\lambda^2\mathcal{K}_0 - 4\delta_1\lambda\mathcal{K}_2\mu\Pi^2 - 2\delta_2\lambda\mathcal{K}_2\Pi^2 -\\
& 2\delta_1\lambda\mathcal{K}_0^2 - 4\kappa\mathcal{K}_2\mu\Pi^2 - 2\kappa\mathcal{K}_2\Pi^2 - 2\kappa\mathcal{K}_0^2 - 4\delta_1\lambda\mathcal{K}_1\mathcal{R}_1 - 4\delta_1\lambda\mathcal{K}_2\mathcal{R}_2 - 4\kappa\mathcal{K}_1\mathcal{R}_1 -\\
& 4\kappa\mathcal{K}_2\mathcal{R}_2 - 4\delta_1\lambda\mu\mathcal{R}_2\varrho^2 - 2\delta_2\lambda\mathcal{R}_2\varrho^2 - 4\kappa\mu\mathcal{R}_2\varrho^2 - 2\kappa\mathcal{R}_2\varrho^2 = 0,\\
\left(\frac{\mathcal{G}'}{\mathcal{G}^2}\right)^{4}: & -12\delta_1\lambda\mathcal{K}_2\mu\varrho^2 - 6\delta_2\lambda\mathcal{K}_2\varrho^2 - 2\delta_1\lambda\mathcal{K}_2^2 - 12\kappa\mathcal{K}_2\mu\varrho^2 - 6\kappa\mathcal{K}_2\varrho^2 - 2\kappa\mathcal{K}_2^2 = 0,\\
\left(\frac{\mathcal{G}'}{\mathcal{G}^2}\right)^{3}: & -4\delta_1\lambda\mathcal{K}_1\mu\varrho^2 - 2\delta_2\lambda\mathcal{K}_1\varrho^2 - 4\delta_1\lambda\mathcal{K}_1\mathcal{K}_2 - 4\kappa\mathcal{K}_1\mu\varrho^2 - 2\kappa\mathcal{K}_1\varrho^2 - 4\kappa\mathcal{K}_1\mathcal{K}_2 = 0,\\
\left(\frac{\mathcal{G}'}{\mathcal{G}^2}\right)^{2}: & -2\alpha^2\gamma\mathcal{K}_2 + 3\alpha^2\delta_2\lambda\mathcal{K}_2 + \alpha^2\kappa\mathcal{K}_2 + 4\alpha\gamma\kappa\mathcal{K}_2 + 4\alpha\lambda^2\mathcal{K}_2 - 16\delta_1\lambda\mathcal{K}_2\mu\Pi\varrho - 8\delta_2\lambda\mathcal{K}_2\Pi\varrho - 2\delta_1\lambda\mathcal{K}_1^2 -\\
& 4\delta_1\lambda\mathcal{K}_0\mathcal{K}_2 - 16\kappa\mathcal{K}_2\mu\Pi\varrho - 8\kappa\mathcal{K}_2\Pi\varrho - 2\kappa\mathcal{K}_1^2 - 4\kappa\mathcal{K}_0\mathcal{K}_2 = 0,\\
\left(\frac{\mathcal{G}'}{\mathcal{G}^2}\right)^{1}: & -2\alpha^2\gamma\mathcal{K}_1 + 3\alpha^2\delta_2\lambda\mathcal{K}_1 + \alpha^2\kappa\mathcal{K}_1 + 4\alpha\gamma\kappa\mathcal{K}_1 + 4\alpha\lambda^2\mathcal{K}_1 - 4\delta_1\lambda\mathcal{K}_1\mu\Pi\varrho - 2\delta_2\lambda\mathcal{K}_1\Pi\varrho -\\
& 4\delta_1\lambda\mathcal{K}_0\mathcal{K}_1 - 4\kappa\mathcal{K}_1\mu\Pi\varrho - 2\kappa\mathcal{K}_1\Pi\varrho - 4\kappa\mathcal{K}_0\mathcal{K}_1 - 4\delta_1\lambda\mathcal{K}_2\mathcal{R}_1 - 4\kappa\mathcal{K}_2\mathcal{R}_1 = 0.
\end{cases} \tag{39}$$

The results obtained from solving these equations are obtained as Family 1 and Family 2.

Family-I:

$$\begin{cases}
\mathcal{K}_0 = -\frac{6\Pi\varrho(2\delta_1\lambda\mu+\delta_2\lambda+2\kappa\mu+\kappa)}{\delta_1\lambda+\kappa},\ \mathcal{K}_1 = 0,\ \mathcal{K}_2 = -\frac{3\varrho^2(2\delta_1\lambda\mu+\delta_2\lambda+2\kappa\mu+\kappa)}{\delta_1\lambda+\kappa},\ \mathcal{R}_1 = 0,\\
\mathcal{R}_2 = -\frac{3\Pi^2(2\delta_1\lambda\mu+\delta_2\lambda+2\kappa\mu+\kappa)}{\delta_1\lambda+\kappa},\\
\alpha = -\frac{2\left(-\sqrt{4\Pi\varrho(2\gamma-3\delta_2\lambda-\kappa)(2\delta_1\lambda\mu+\delta_2\lambda+2\kappa\mu+\kappa)+(\gamma\kappa+\lambda^2)^2}+\gamma\kappa+\lambda^2\right)}{-2\gamma+3\delta_2\lambda+\kappa}.
\end{cases} \tag{40}$$

Then the various types of solutions of Equation (19) are obtained as follows:

- **Trigonometric solution:** When $\Pi\varrho > 0$, then the Equation (16) has the solution as:

$$\Theta_1(x,t) = \left[-\frac{3\left(c_1^2+c_2^2\right)^2\Pi\varrho\left(2\delta_1\lambda\mu+\delta_2\lambda+2\kappa\mu+\kappa\right)}{\left(\delta_1\lambda+\kappa\right)\left(c_1\sin\left(\chi\sqrt{\Pi\varrho}\right)-c_2\cos\left(\chi\sqrt{\Pi\varrho}\right)\right)^2\left(c_2\sin\left(\chi\sqrt{\Pi\varrho}\right)+c_1\cos\left(\chi\sqrt{\Pi\varrho}\right)\right)^2}\right]\times e^{i(\alpha(\gamma t+x))}. \tag{41}$$

• **Hyperbolic solution:** When $\Pi\varrho < 0$, then the Equation (16) has the solution as:

$$\Theta_2(x,t) = \left[\frac{3\Pi\left(2\delta_1\lambda\mu+\delta_2\lambda+2\kappa\mu+\kappa\right)\left(-\frac{\varrho^2\left(c_1\left(\sinh\left(2\chi\sqrt{\Pi\varrho}\right)+\cosh\left(2\chi\sqrt{\Pi\varrho}\right)\right)+c_2\right)^2}{\left(c_2-c_1\left(\sinh\left(2\chi\sqrt{\Pi\varrho}\right)+\cosh\left(2\chi\sqrt{\Pi\varrho}\right)\right)\right)^2}-\frac{\left(c_2-c_1\left(\sinh\left(2\chi\sqrt{\Pi\varrho}\right)+\cosh\left(2\chi\sqrt{\Pi\varrho}\right)\right)\right)^2}{\left(c_1\left(\sinh\left(2\chi\sqrt{\Pi\varrho}\right)+\cosh\left(2\chi\sqrt{\Pi\varrho}\right)\right)+c_2\right)^2}-2\varrho\right)}{\delta_1\lambda+\kappa}\right]\times e^{i(\alpha(\gamma t+x))}. \quad (42)$$

• **Rational solution:** When $\Pi \neq 0,\ \varrho = 0$, then the Equation (16) has the solution as:

$$\Theta_3(x,t) = \left[-\frac{3\left(c_1^2\left(\chi^2\Pi\varrho+1\right)+2c_2c_1\chi\Pi\varrho+c_2^2\Pi\varrho\right)^2\left(2\delta_1\lambda\mu+\delta_2\lambda+2\kappa\mu+\kappa\right)}{c_1^2\left(c_1\chi+c_2\right)^2\left(\delta_1\lambda+\kappa\right)}\right]\times e^{i(\alpha(\gamma t+x))}. \quad (43)$$

Family-II:

$$\begin{cases}\mathcal{K}_0 = \frac{4\alpha\mu\Pi\varrho\left(-\kappa(\alpha+4\gamma)+2\alpha\gamma-3\alpha\delta_2\lambda-4\lambda^2\right)}{\delta_2\lambda(16\Pi\varrho-3\alpha^2)+\alpha(-\kappa(\alpha+4\gamma)+2\alpha\gamma-4\lambda^2)+16\kappa\Pi\varrho},\ \mathcal{K}_1 = 0,\ \mathcal{K}_2 = \frac{6\alpha\mu\varrho^2\left(\alpha(\kappa-2\gamma)+3\alpha\delta_2\lambda+4\left(\gamma\kappa+\lambda^2\right)\right)}{\delta_2\lambda(16\Pi\varrho-3\alpha^2)+\alpha(-\kappa(\alpha+4\gamma)+2\alpha\gamma-4\lambda^2)+16\kappa\Pi\varrho},\\ \mathcal{R}_1 = 0,\ \mathcal{R}_2 = \frac{6\alpha\mu\Pi^2\left(\alpha(\kappa-2\gamma)+3\alpha\delta_2\lambda+4\left(\gamma\kappa+\lambda^2\right)\right)}{\delta_2\lambda(16\Pi\varrho-3\alpha^2)+\alpha(-\kappa(\alpha+4\gamma)+2\alpha\gamma-4\lambda^2)+16\kappa\Pi\varrho},\ \delta_1 = \frac{\alpha^2(\kappa-2\gamma)+\delta_2\lambda\left(3\alpha^2-16\Pi\varrho\right)+4\alpha\left(\gamma\kappa+\lambda^2\right)-16\kappa(2\mu+1)\Pi\varrho}{32\lambda\mu\Pi\varrho}.\end{cases} \quad (44)$$

• **Trigonometric solution:** When $\Pi\varrho > 0$, then the Equation (16) has the solution as:

$$\begin{cases}\Theta_4(x,t) = \left[-\frac{2\alpha\mu\Pi\varrho\left(\alpha(2\gamma-\kappa)-3\alpha\delta_2\lambda-4\left(\gamma\kappa+\lambda^2\right)\right)\left(4c_2c_1^3\sin\left(4\chi\sqrt{\Pi\varrho}\right)-4c_2^3c_1\sin\left(4\chi\sqrt{\Pi\varrho}\right)+c_1^4\left(\cos\left(4\chi\sqrt{\Pi\varrho}\right)+2\right)-2c_2^2c_1^2\left(3\cos\left(4\chi\sqrt{\Pi\varrho}\right)-2\right)+c_2^4\left(\cos\left(4\chi\sqrt{\Pi\varrho}\right)+2\right)\right)}{\left(c_1\sin\left(\chi\sqrt{\Pi\varrho}\right)-c_2\cos\left(\chi\sqrt{\Pi\varrho}\right)\right)^2\left(c_2\sin\left(\chi\sqrt{\Pi\varrho}\right)+c_1\cos\left(\chi\sqrt{\Pi\varrho}\right)\right)^2\left(\alpha^2(2\gamma-\kappa)+\delta_2\left(16\lambda\Pi\varrho-3\alpha^2\lambda\right)-4\alpha\left(\gamma\kappa+\lambda^2\right)+16\kappa\Pi\varrho\right)}\right]\\ \times e^{i(\alpha(x+\gamma t))}.\end{cases} \quad (45)$$

• **Hyperbolic solution:** When $\Pi\varrho < 0$, then the Equation (16) has the solution as:

$$\begin{cases}\Theta_5(x,t) = \left[\frac{2\alpha\mu\Pi\left(2\varrho\left(-\kappa(\alpha+4\gamma)+2\alpha\gamma-3\alpha\delta_2\lambda-4\lambda^2\right)-\frac{3\varrho^2\left(\alpha(2\gamma-\kappa)-3\alpha\delta_2\lambda-4\left(\gamma\kappa+\lambda^2\right)\right)\left(c_1\left(\sinh\left(2\chi\sqrt{\Pi\varrho}\right)+\cosh\left(2\chi\sqrt{\Pi\varrho}\right)\right)+c_2\right)^2}{\left(c_2-c_1\left(\sinh\left(2\chi\sqrt{\Pi\varrho}\right)+\cosh\left(2\chi\sqrt{\Pi\varrho}\right)\right)\right)^2}\right)}{\delta_2\lambda\left(16\Pi\varrho-3\alpha^2\right)+\alpha\left(-\kappa(\alpha+4\gamma)+2\alpha\gamma-4\lambda^2\right)+16\kappa\Pi\varrho}\right.\\ \left.-\frac{6\alpha\mu\Pi\varrho^2\left(\alpha(2\gamma-\kappa)-3\alpha\delta_2\lambda-4\left(\gamma\kappa+\lambda^2\right)\right)\left(c_1\left(\sinh\left(2\chi\sqrt{\Pi\varrho}\right)+\cosh\left(2\chi\sqrt{\Pi\varrho}\right)\right)+c_2\right)^2}{\left(c_2-c_1\left(\sinh\left(2\chi\sqrt{\Pi\varrho}\right)+\cosh\left(2\chi\sqrt{\Pi\varrho}\right)\right)\right)^2}}{\delta_2\lambda\left(16\Pi\varrho-3\alpha^2\right)+\alpha\left(-\kappa(\alpha+4\gamma)+2\alpha\gamma-4\lambda^2\right)+16\kappa\Pi\varrho}\right]\times e^{i(\alpha(x+\gamma t))}.\end{cases} \quad (46)$$

• **Rational solution:** When $\Pi \neq 0,\ \varrho = 0$, then the Equation (16) has the solution as:

$$\begin{cases}\Theta_6(x,t) = \left[-\frac{2\alpha\mu\left(4c_2c_1^3\chi\Pi\varrho\left(3\chi^2\Pi\varrho-1\right)+2c_2^2c_1^2\Pi\varrho\left(9\chi^2\Pi\varrho-1\right)+c_1^4\left(3\chi^4\Pi^2\varrho^2-2\chi^2\Pi\varrho+3\right)+12c_2^3c_1\chi\Pi^2\varrho^2+3c_2^4\Pi^2\varrho^2\right)}{c_1^2(c_1\chi+c_2)^2\left(\alpha^2(2\gamma-\kappa)+\delta_2\left(16\lambda\Pi\varrho-3\alpha^2\lambda\right)-4\alpha\left(\gamma\kappa+\lambda^2\right)+16\kappa\Pi\varrho\right)}\right]\\ \left(\alpha(2\gamma-\kappa)-3\alpha\delta_2\lambda-4\left(\gamma\kappa+\lambda^2\right)\right)\times e^{i(\alpha(x+\gamma t))}.\end{cases} \quad (47)$$

For each of the previous solutions $\chi = x - \kappa t$.

5. The Graphical Visualization and Physical Interpretation

To gain deeper insight into the dynamical characteristics and propagation features of the obtained soliton solutions, we provide a comprehensive graphical analysis of the solution profiles derived in this study. The figures demonstrate the behavior of the dual-mode wave solutions under the influence of both the square-root Kerr nonlinearity and Bohm-type quantum potential within the resonant nonlinear Schrödinger framework. Various visualization tools are utilized, including 3D surface plots, contour projections, and 2D amplitude profiles.

Relation with experimental observations.. Although the present work is theoretical in nature, the obtained optical soliton profiles are qualitatively consistent with experimentally observed nonlinear pulse structures in optical fibers and related photonic systems. In particular, the bright and localized waveforms shown in Figures (1–4) resemble soliton behaviors reported in nonlinear optical fibers, where stable pulse propagation results from the balance between dispersion and Kerr-type nonlinear effects. The square-root Kerr response considered in the present model can be viewed as an effective saturable nonlinear mechanism relevant to some nonlinear optical media and semiconductor waveguides. Therefore,

while the present study does not include direct experimental measurements, the derived exact solutions provide a meaningful analytical framework for interpreting experimentally observed pulse localization, waveform preservation, and nonlinear pulse shaping in practical optical transmission environments [44, 45, 46]. The numerical parameter values used in the graphical simulations are selected within physically reasonable ranges to illustrate different nonlinear wave regimes and do not correspond to a specific experimental setup.

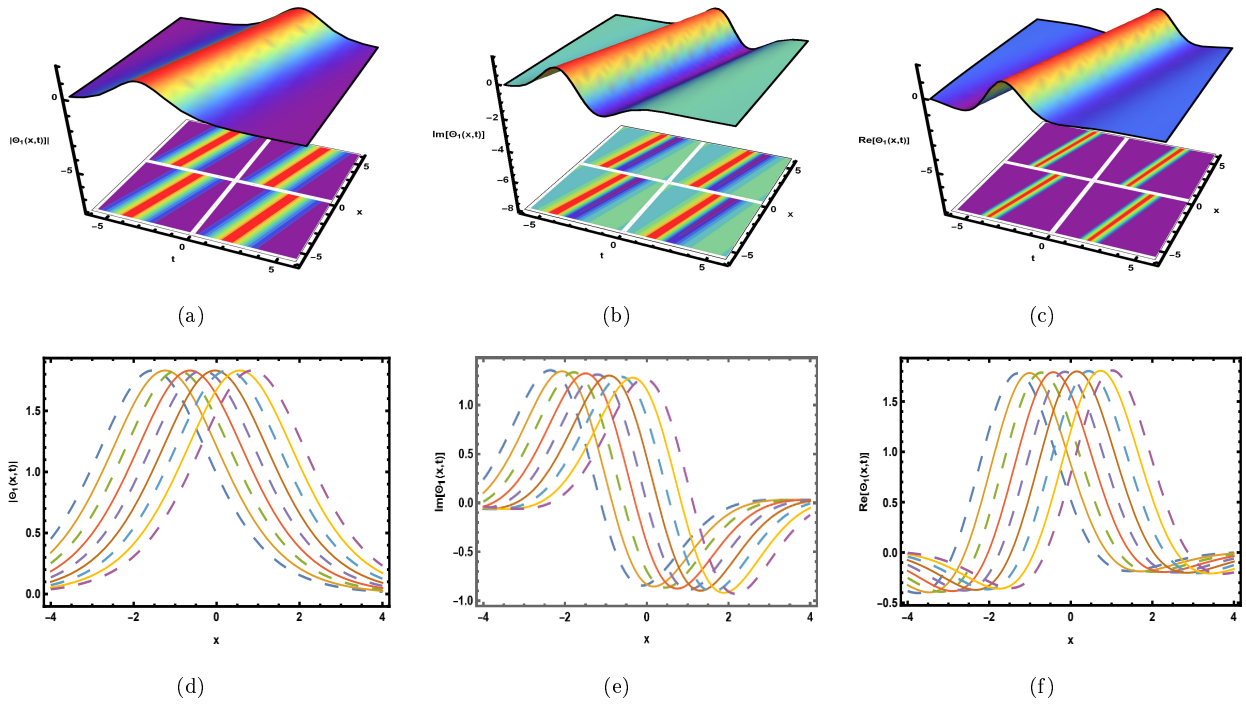


Figure 1: The visualization of the solution (23) for $\phi = -0.29,\ \alpha = -0.9,\ \kappa = 0.3,\ \mu = 0.49,\ \lambda = 0.33,\ \delta_1 = 0.3,\ \delta_2 = 0.45,\ \pi_0 = 0.34$.

Figure 1 represents the graphical behavior of the exact bright soliton solution $\Theta(x,t)$ corresponding to Equation (23), under the selected parameter values: $\phi = -0.29$, $\alpha = -0.9$, $\kappa = 0.3$, $\mu = 0.49$, $\lambda = 0.33$, $\delta_1 = 0.3$, $\delta_2 = 0.45$, and $\pi_0 = 0.34$. Subfigures (1(a))–(1(c)) visualize the three-dimensional surfaces and density contours of the modulus $|\Theta|$, the imaginary part $\mathrm{Im}[\Theta]$, and the real part $\mathrm{Re}[\Theta]$, respectively. These plots show smooth, bell-shaped bright solitons that exhibit strong spatial localization and robustness across both spatial and temporal domains. The contribution of the Bohm-type quantum potential and the square root Kerr nonlinearity is evident in the formation of confined, localized structures, which are physically relevant for modeling wave propagation in nonlinear optical media. Subfigures (1(d))–(1(f)) present two-dimensional line plots of the corresponding quantities over a range of spatial coordinates, further emphasizing the temporal coherence and translational invariance of the soliton profile. The solution's persistence in shape and amplitude validates its potential applications in nonlinear fiber optics, quantum communication systems, and ultrafast signal processing.

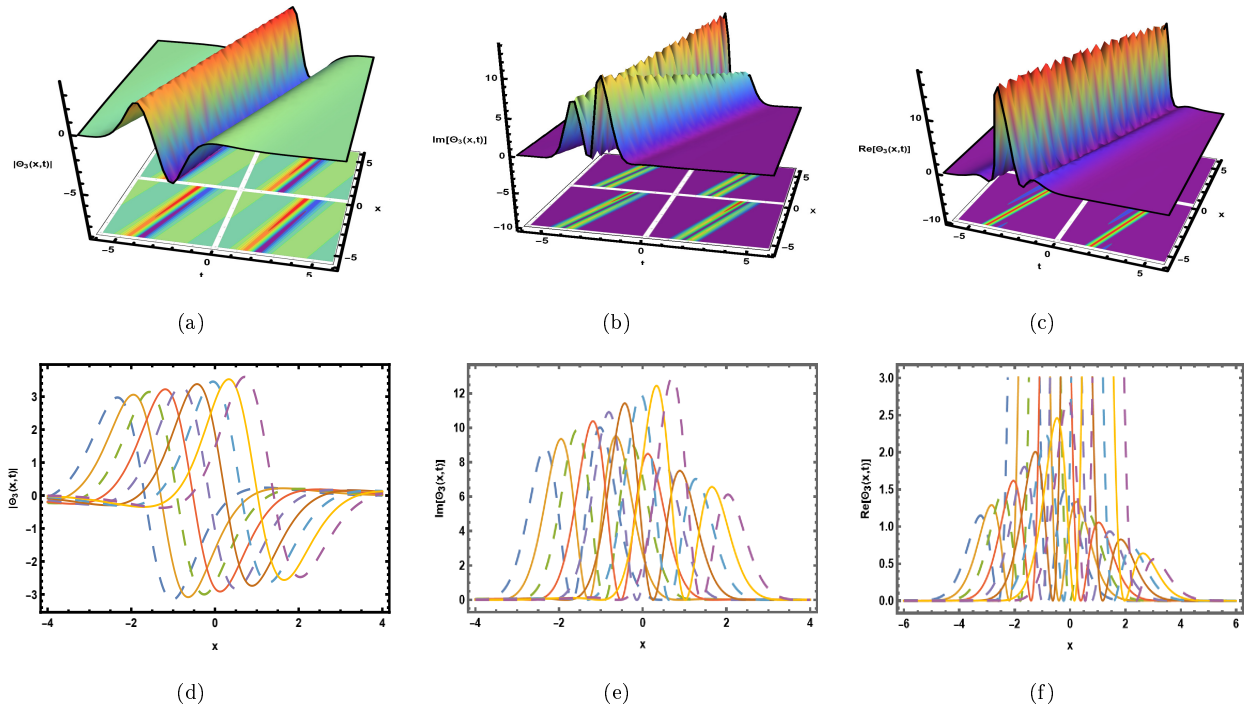


Figure 2: The visualization of the solution (25) for $\phi = -0.3$, $\alpha = -0.8$, $\kappa = 0.35$, $\mu = 0.59$, $\lambda = 0.32$, $\delta_1 = 0.33$, $\delta_2 = 0.55$, $\pi_0 = 0.24$, $\epsilon = 1$.

Figure 2 displays the graphical interpretation of the complex-valued solution $\Theta(x,t)$ provided in Equation (25), under the parameter regime $\phi = -0.3$, $\alpha = -0.8$, $\kappa = 0.35$, $\mu = 0.59$, $\lambda = 0.32$, $\delta_1 = 0.33$, $\delta_2 = 0.55$, $\pi_0 = 0.24$, and $\epsilon = 1$. Subfigures (2(a))–(2(c)) demonstrate the three-dimensional and contour visualizations of the modulus $|\Theta|$, imaginary part $\mathrm{Im}[\Theta]$, and real part $\mathrm{Re}[\Theta]$, respectively. The solution reveals a mixed or combo wave profile exhibiting oscillatory and kink-type features. Particularly, the modulus shows sharp transitions indicating a composite behavior combining bright and dark-like components. The imaginary part shows rapid localized peaks, while the real part exhibits high-frequency oscillations, implying strong modulation effects governed by the Bohm potential and square root Kerr-type nonlinearity. In the two-dimensional plots (2(d))–(2(f)), we analyze multiple lobes and interference patterns in the spatial distribution, suggesting nonlinear wave interactions. These dynamics are highly sensitive to the choice of phase velocity λ, nonlinearity parameter α, and quantum correction μ, all of which play a significant role in tailoring localized structures. Such solutions may find utility in optical pulse shaping, nonlinear waveguides, and coherent light-matter interactions, where precise control over wave shape and intensity is significant. The sharp oscillatory features observed in certain regions of the wave profiles are a consequence of the nonlinear interaction between the square-root Kerr response and the Bohm-type quantum potential, and their intensity can be controlled through appropriate selection of the model parameters.

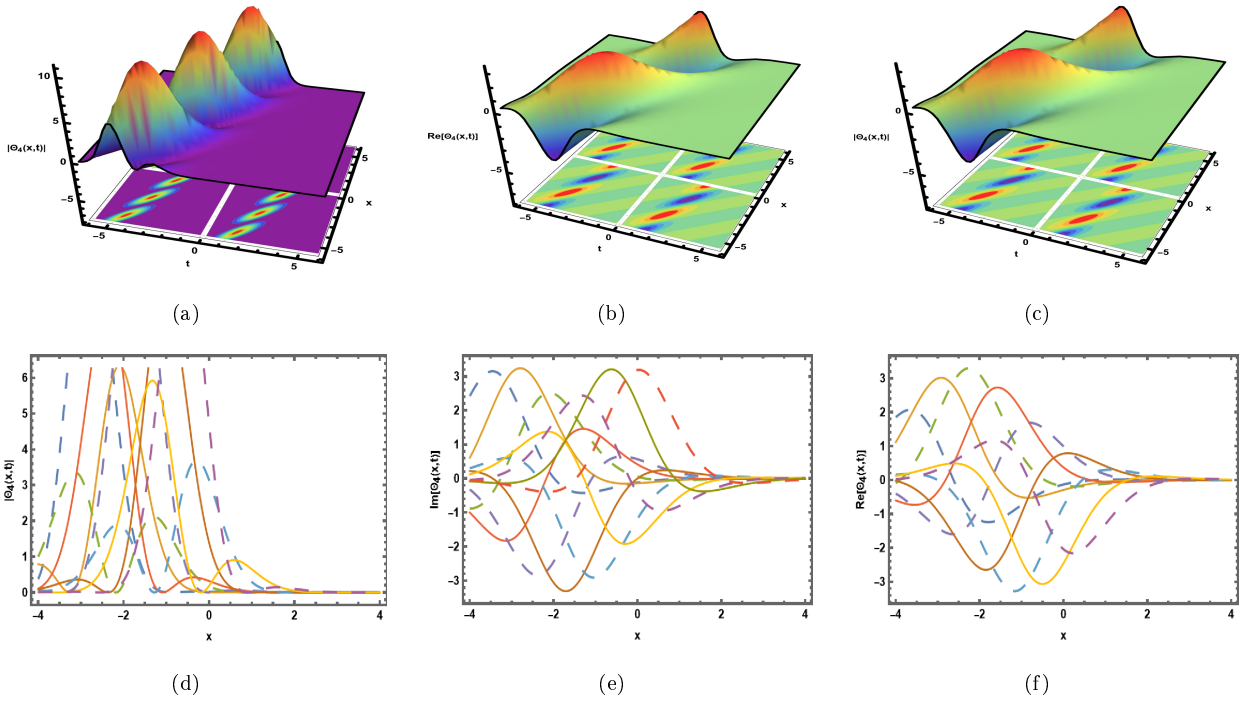


Figure 3: The visualization of the solution (26) for $\phi = -0.51,\ \alpha = 0.91,\ \kappa = 0.31,\ \mu = 0.45,\ \lambda = 0.35,\ \delta_1 = 0.25,\ \delta_2 = 0.55,\ \pi_0 = 0.44$.

Figure 3 demonstrates the dynamics of the solution $\Theta(x,t)$ given by Equation (26) under the influence of the parameter set $\phi = -0.51$, $\alpha = 0.91$, $\kappa = 0.31$, $\mu = 0.45$, $\lambda = 0.35$, $\delta_1 = 0.25$, $\delta_2 = 0.55$, and $\pi_0 = 0.44$. Subplots (3(a))–(3(c)) show the three-dimensional evolution of $|\Theta|$, $\mathrm{Re}[\Theta]$, and $\mathrm{Im}[\Theta]$, respectively. The behavior of $|\Theta|$ in panel (3(a)) indicates a sequence of localized sharp pulses, resembling rogue-wave-like formations in nonlinear optical contexts, such as high-intensity bursts in fiber communications or plasma waves. In the corresponding two-dimensional projections shown in subplots (3(d))–(3(f)), the amplitude profiles show significant amplitude amplification followed by decay, confirming energy localization in specific space-time regions. The real and imaginary parts demonstrate oscillatory behavior with nonuniform envelope widths, which is largely attributed to the combined effects of the square-root Kerr nonlinearity (influenced by α) and quantum corrections via the Bohm-type potential (governed by μ). The results point to potential utility in applications such as wave energy localization, nonlinear signal processing, and coherent matter-wave dynamics in quantum optics and Bose–Einstein condensates.

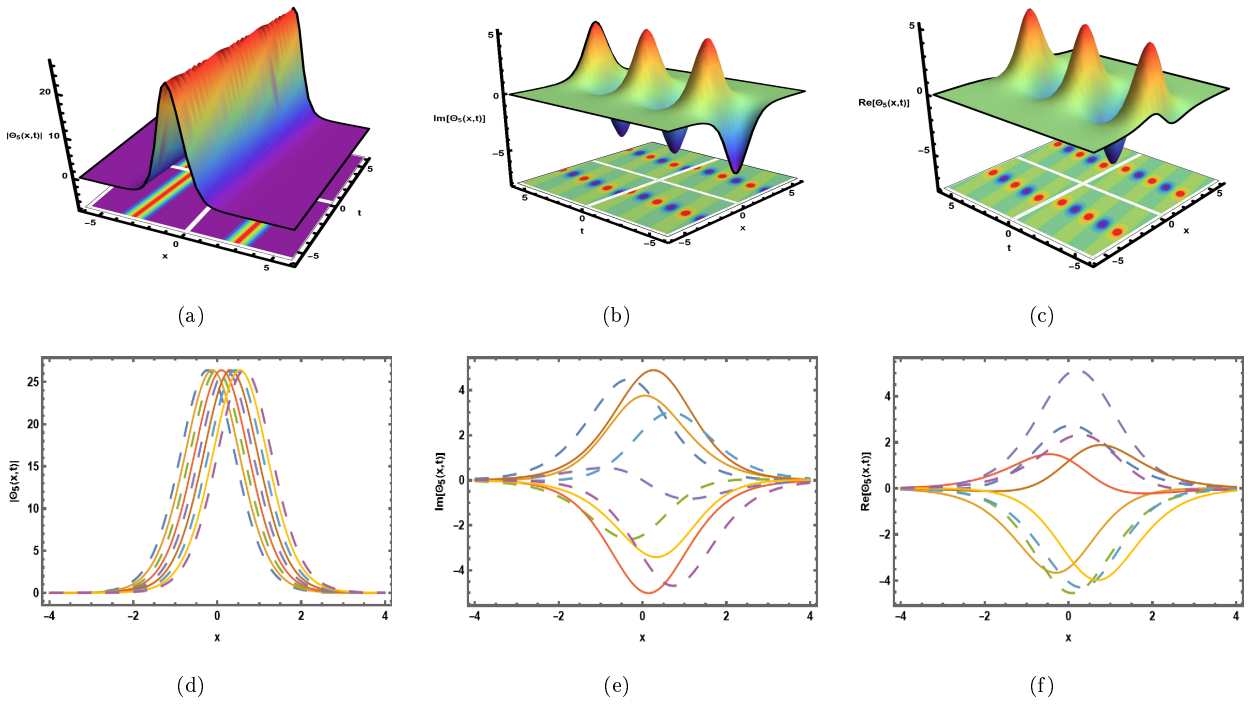


Figure 4: The visualization of the solution (27) for $\phi = -0.59,\ \alpha = -0.23,\ \kappa = 0.11,\ \mu = 0.65,\ \lambda = 0.25,\ \delta_1 = 0.24,\ \delta_2 = 0.65,\ \pi_0 = 0.24$.

Figure 4 illustrates the wave dynamics relating to the solution in Equation (27) for the parameter configuration $\phi = -0.59$, $\alpha = -0.23$, $\kappa = 0.11$, $\mu = 0.65$, $\lambda = 0.25$, $\delta_1 = 0.24$, $\delta_2 = 0.65$, and $\pi_0 = 0.24$. In subplot (4(a)), the amplitude $|\Theta(x,t)|$ shows a sharply localized and high-intensity structure resembling a high-order bright soliton, which is a significant feature in nonlinear optical communication systems, particularly for optical pulse compression and signal focusing. Subplots (4(b)) and (4(c)) present the imaginary and real components, which reflect periodic interactions and localized oscillatory patterns, revealing modulation instability effects. The corresponding 2D plots (4(d))–(4(f)) highlight the enhanced sharpness and symmetry in the amplitude profile, while the real and imaginary parts of the wavefield exhibit smooth transitions and dispersion-dominated tails. The large value of the quantum potential coefficient μ emphasizes the Bohm-type dispersive influence, resulting in amplified spatial gradients. Such profiles are particularly relevant in contexts such as nonlinear metamaterials, photonic crystal modeling, and structured light waveguides where wave steepening and localization are advantageous.

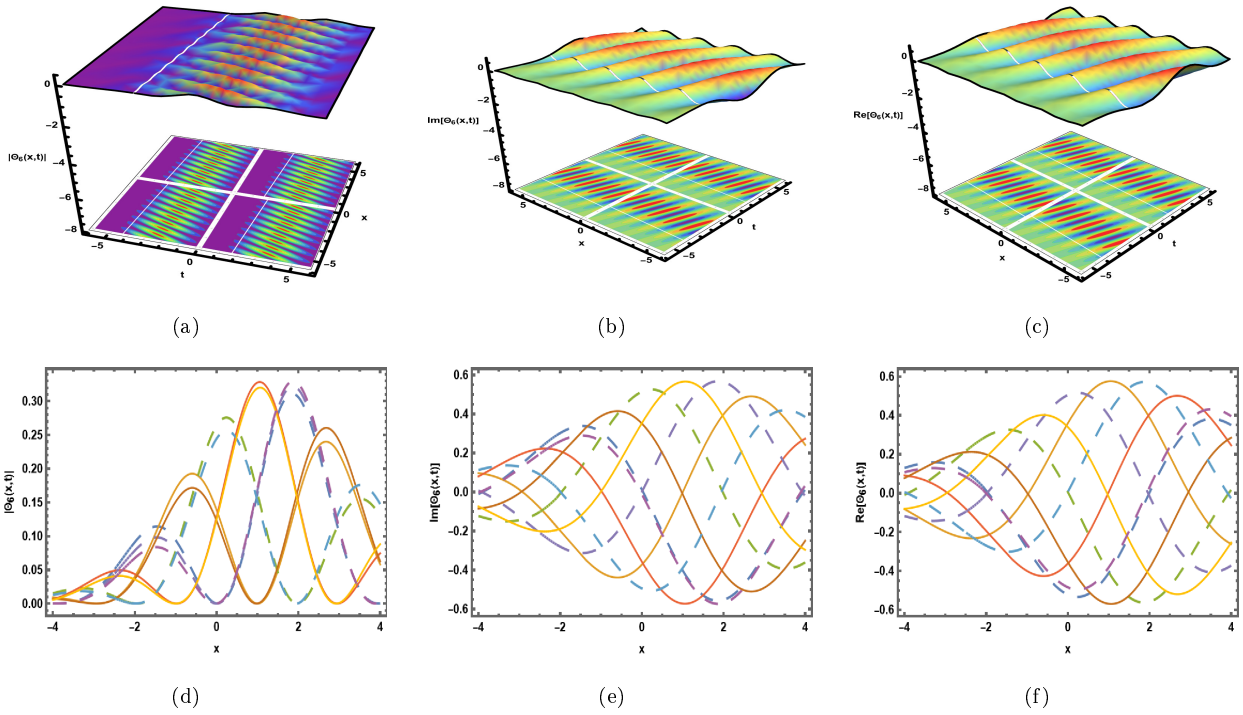


Figure 5: The visualization of the solution (28) for $\phi = -0.7,\ \alpha = -0.8,\ \kappa = 0.35,\ \mu = 0.59,\ \lambda = 1.9,\ \delta_1 = 0.33,\ \delta_2 = 0.55,\ \pi_0 = 0.44,\ \epsilon = 1,\ f_1 = 7,\ f_2 = 8.$

Figure 5 indicates the solution behavior of Equation (28) for the parameter configuration $\phi = -0.7$, $\alpha = -0.8$, $\kappa = 0.35$, $\mu = 0.59$, $\lambda = 1.9$, $\delta_1 = 0.33$, $\delta_2 = 0.55$, $\pi_0 = 0.44$, $\epsilon = 1$, $f_1 = 7$, and $f_2 = 8$. The 3D plots (5(a))–(5(c)) clearly show periodic modulated wave structures, where both the amplitude and real/imaginary components display low-intensity, wave packet-like oscillations. This structure stems from the high phase velocity λ and frequency parameters f_1 and f_2, resulting in a relatively smooth, bounded solution profile. In 2D visualizations (5(d))–(5(f)), the amplitude $|\Theta(x,t)|$ remains within a small range, showcasing an interference-like envelope with modulated crests, indicating coherent pulse behaviors of low peak power important for waveguides and fiber-optic systems operating under weakly nonlinear regimes. The imaginary and real components are nearly symmetric and display well-defined harmonic features, highlighting the contribution of dual-mode wave interaction and tunable dispersive behavior through μ and δ_1, δ_2. These features suggest potential utility in optical switching, pulse shaping, and weak nonlinear photonics applications.

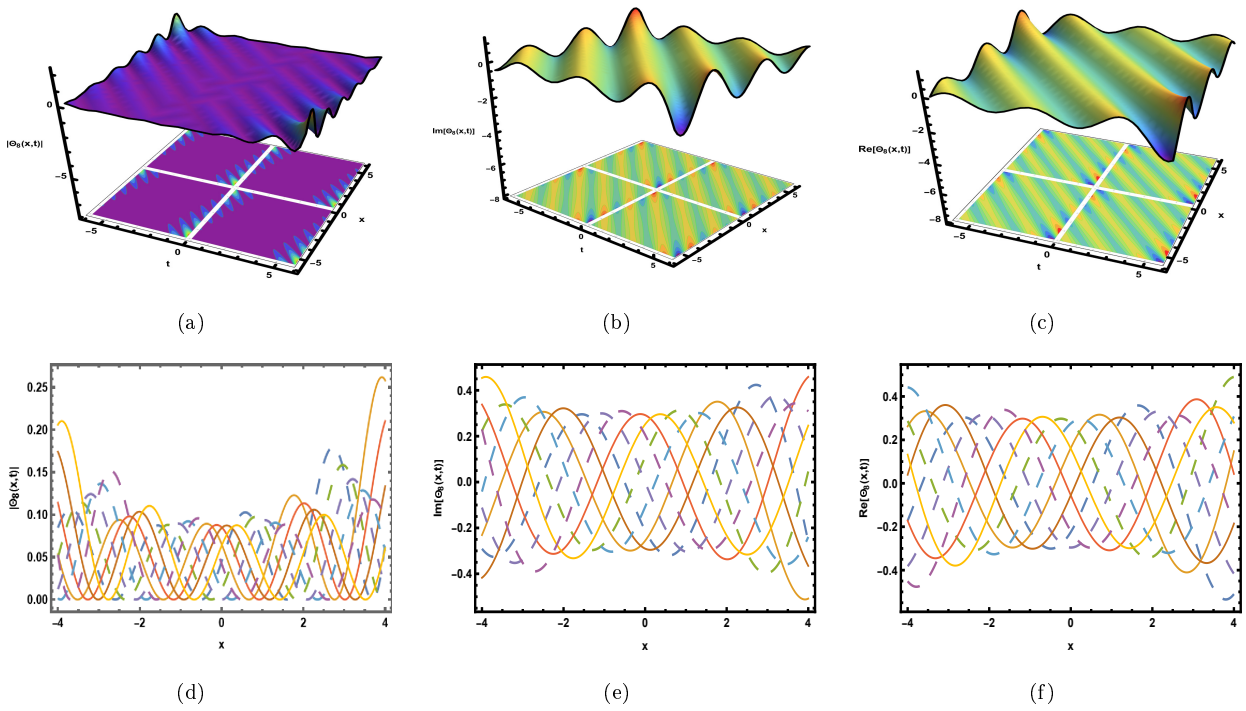


Figure 6: The visualization of the solution (30) for $\phi = 0.02,\ \alpha = 1.5,\ \kappa = 0.3,\ \mu = 1.9,\ \lambda = 0.33,\ \delta_1 = 0.3,\ \delta_2 = 0.45,\ \pi_0 = 0.24$.

Figure 6 represents the graphical profiles of the solution (30) under the parameter set $\phi = 0.02$, $\alpha = 1.5$, $\kappa = 0.3$, $\mu = 1.9$, $\lambda = 0.33$, $\delta_1 = 0.3$, $\delta_2 = 0.45$, and $\pi_0 = 0.24$. The three-dimensional plots (6(a))–(6(c)) reveal a strongly modulated periodic wave structure. Specifically, the real and imaginary components display sustained, symmetric wave patterns due to the relatively high dispersion coefficient μ and enhanced nonlinear feedback introduced by α and λ. The amplitude plot in subfigure (6(d)) demonstrates low-intensity oscillations with gradually varying peaks, indicative of periodic wave packets with spatial modulation. The imaginary and real parts in subfigures (6(e)) and (6(f)) show harmonic waveforms over a finite domain, maintaining a consistent frequency across the range $x \in [-4, 4]$. This type of pattern corresponds to periodic breathers and modulated continuous waves-highly relevant in nonlinear optics for pulse train generation, optical frequency combs, and coherent light propagation in photonic crystals or metamaterials. The fine-tuned balance of parameters controls the periodicity and amplitude, offering tunability in practical wave-based systems.

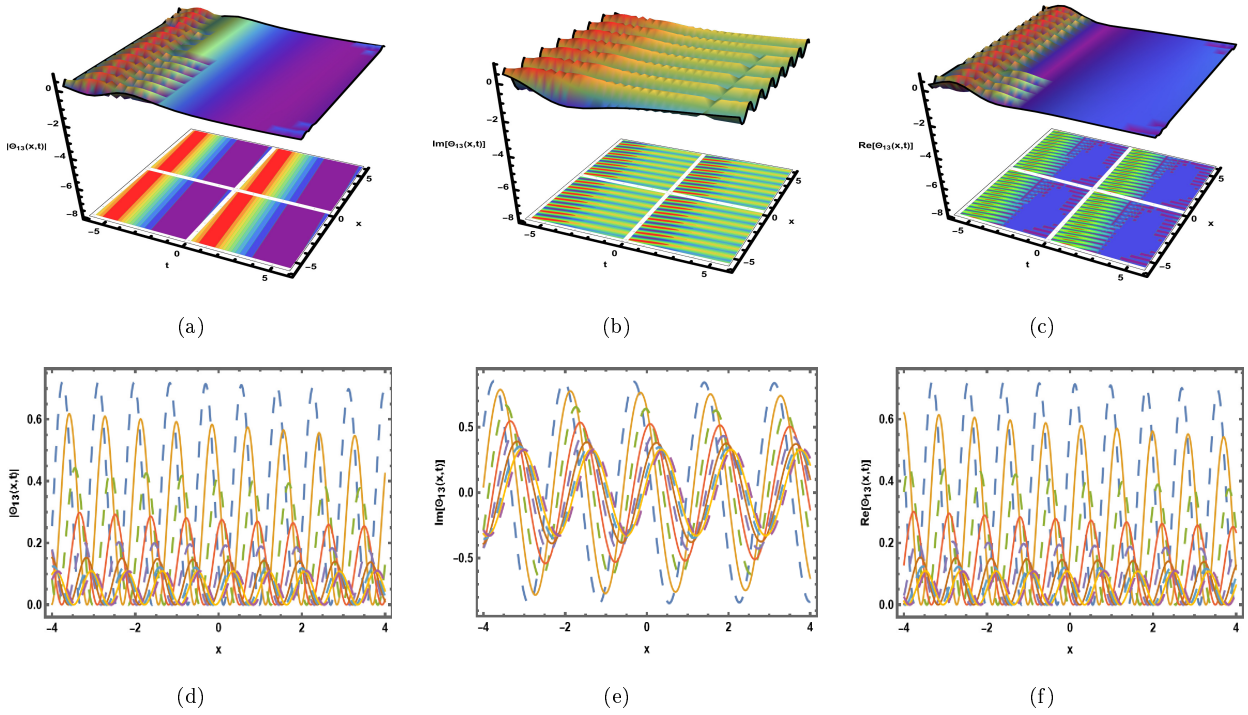


Figure 7: The visualization of the solution (35) for $\phi = 0.04,\ \alpha = -0.05,\ \kappa = -0.06,\ \mu = 0.06,\ \lambda = 2,\ \delta_1 = 0.22,\ \delta_2 = 0.85,\ \pi_0 = 0.44,\ \epsilon = 1,\ f_1 = 4,\ f_2 = 9$.

Figure 7 represents the graphical patterns of the solution (35) using the parameter set $\phi = 0.04$, $\alpha = -0.05$, $\kappa = -0.06$, $\mu = 0.06$, $\lambda = 2$, $\delta_1 = 0.22$, $\delta_2 = 0.85$, $\pi_0 = 0.44$, $\epsilon = 1$, $f_1 = 4$, and $f_2 = 9$. Subfigures (7(a))–(7(c)) depict strong trigonometric wave characteristics, visible as periodic stripe-like patterns in both real and imaginary parts. The high values of λ and δ_2 amplify oscillations, whereas the small κ and μ values moderate the wave steepness and spatial frequency. The bottom panels (7(d))–(7(f)) highlight the oscillatory nature of the amplitude, imaginary, and real components of the solution. The plots show periodic crests with regular spacing and amplitude, a hallmark of trigonometric-type behavior governed by sine and cosine function components. These waveforms are especially relevant in the study of nonlinear optical gratings, signal processing, and microwave photonic systems, where such controlled periodicity can be harnessed for wave filtering, harmonic generation, and signal encoding. The combined influence of structural and frequency parameters facilitates tuning the periodic intensity and wavelength of the generated waveforms.

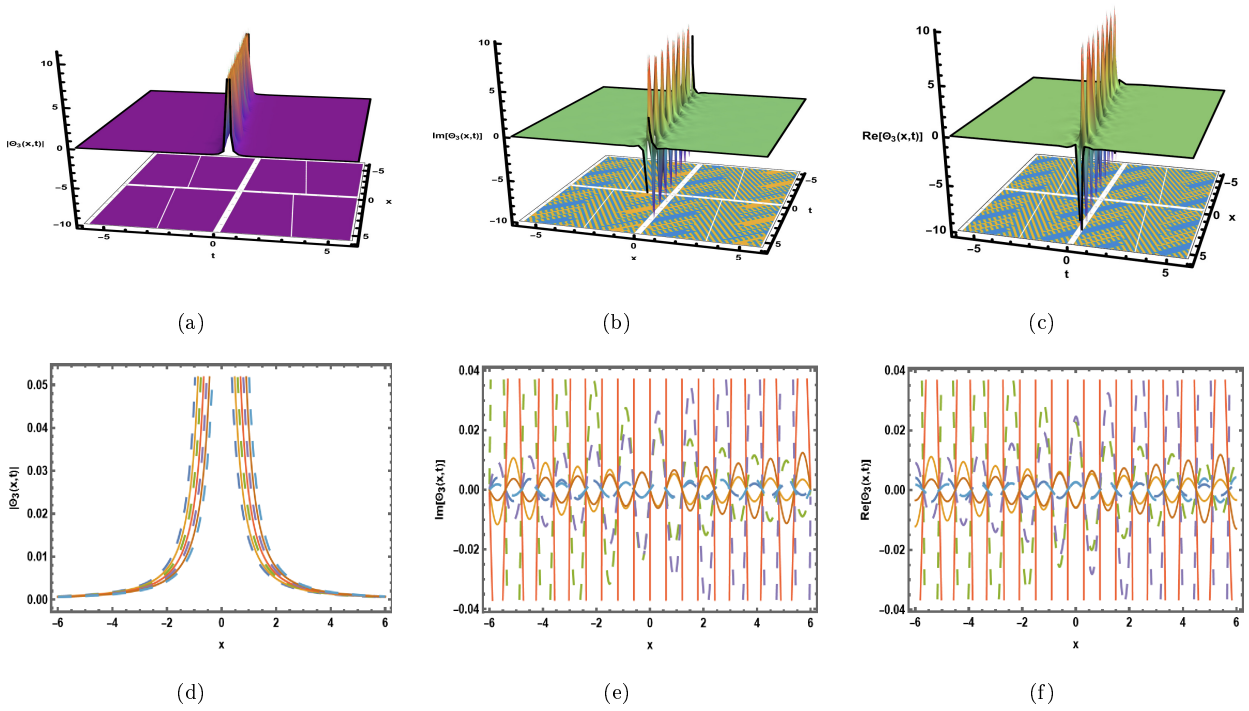


Figure 8: The visualization of the solution (43) for $\Pi = 0,\ \varrho = 0.01,\ \gamma = -1.8,\ \lambda = -0.21,\ c_1 = 5,\ c_2 = 1,\ \alpha = -1.5,\ \delta_2 = 0.1,\ \mu = -0.15,\ \kappa = 9.5$.

Figure 8 demonstrates the visualization of solution (43) corresponding to the parameter set $\Pi = 0$, $\varrho = 0.01$, $\gamma = -1.8$, $\lambda = -0.21$, $c_1 = 5$, $c_2 = 1$, $\alpha = -1.5$, $\delta_2 = 0.1$, $\mu = -0.15$, and $\kappa = 9.5$. Subfigures (8(a))–(8(c)) clearly show rational-type localized structures with sharp peaks around the origin. The amplitude shows a singular behavior that rapidly decays to zero in both spatial and temporal directions. The large value of κ and highly negative γ enhance the singular steepness and compression of the solution in a narrow region. The 2D plots in subfigures (8(d))–(8(f)) signify rational decay characteristics, particularly in the amplitude plot (8(f)), where the function behaves like a sharply peaked pulse centered at $x = 0$. The real and imaginary components (8(d))–(8(f)) oscillate with high frequency and decreasing amplitude, reminiscent of rational-type rogue wave tails. This solution profile is crucial in modeling extreme localized energy pulses, such as rogue waves in deep ocean physics or sharply focused optical beams in nonlinear optics. The rational behavior presented by the given parameters allows simulation of highly localized nonlinear wave interactions under near-singular initial conditions.

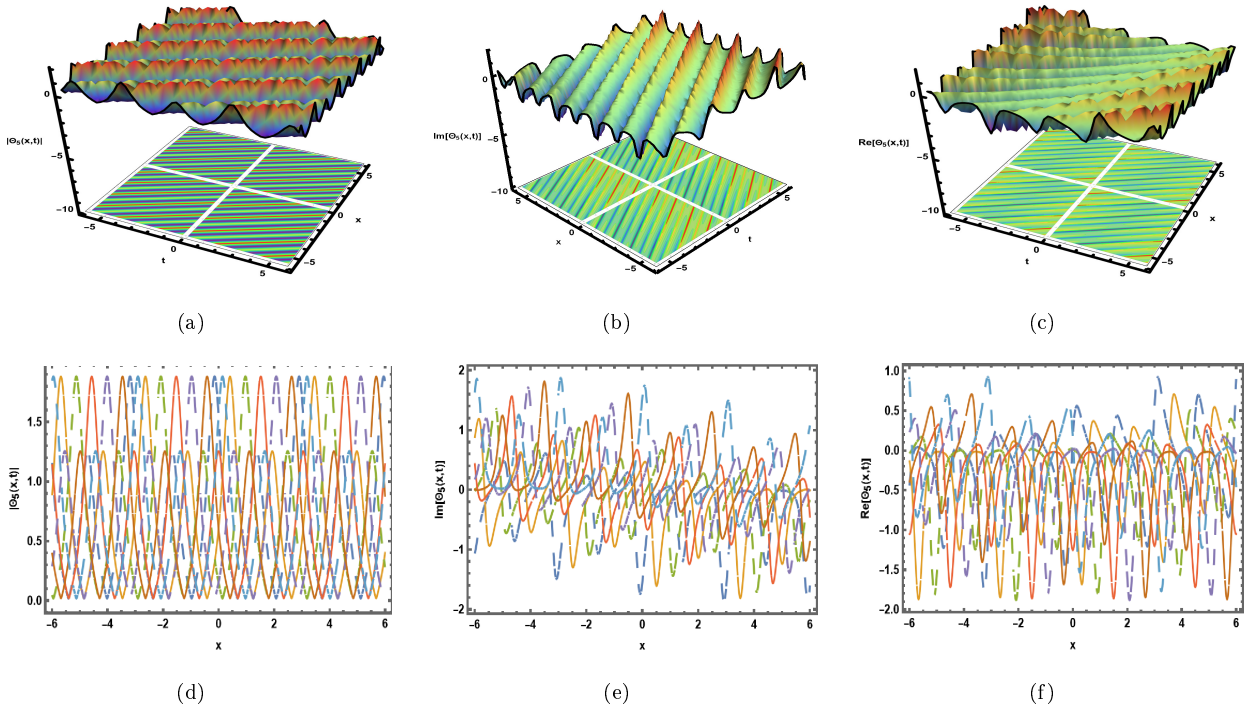


Figure 9: The visualization of the solution (46) for $\Pi = 0.41,\ \varrho = -0.8,\ \gamma = -0.43,\ \lambda = 0.1,\ c_1 = 4,\ c_2 = 2,\ \alpha = -0.33,\ \delta_2 = -0.5,\ \mu = 0.65,\ \kappa = 1.8$.

Figure 9 represents the graphical representation of solution (46) with parameter values $\Pi = 0$, $\varrho = 0.01$, $\gamma = -1.8$, $\lambda = -0.11$, $c_1 = 6$, $c_2 = 1$, $\alpha = -1.5$, $\delta_2 = 0.1$, $\mu = -0.25$, and $\kappa = 10.5$. The surface plots (9(a))–(9(c)) reveal a highly localized and sharply peaked rational structure centered around $x = 0$, $t = 0$. Compared to Figure 9, the amplitude peak is more pronounced due to increased nonlinearity ($\kappa = 10.5$) and deeper negative μ, enhancing singular concentration. Subfigures (9(d))–(9(f)) confirm the rational nature through the behavior of modulus, imaginary, and real parts. The amplitude in (9(d)) resembles a rational pulse that decays symmetrically, while the imaginary and real parts in (9(e)) and (9(f)) exhibit fine oscillations across the spatial domain $x \in [-6, 6]$. These dynamics suggest applications in nonlinear waveguides, optical filamentation, and plasma bursts, where rational solutions are used to represent high-intensity, non-dispersive phenomena governed by certain parameter regimes.

6. Conclusion

In this work, we have explored a dual-mode resonant nonlinear Schrödinger equation (RNLSE) augmented by the Bohm potential and governed by the square root Kerr nonlinearity. Applying two powerful analytical tools the eMETFM and the $\left(\frac{\mathcal{G}'}{\mathcal{G}^2}\right)$-expansion function method we obtained a suite of exact wave solutions. These include hyperbolic, trigonometric, and rational forms, each capturing distinct dynamical wave structures. The application of these methods not only represents their effectiveness in solving nonlinear partial differential equations but also uncovers diverse solution behaviors with direct relevance to dual-mode optical systems, quantum fluid mechanics, and communication engineering. The visual interpretation of solutions through 3D surface plots, contour projections, and 2D profiles provides insight into the physical implications of the derived waveforms, emphasizing localized structures

and dual-wave interactions. The study underscores the interplay between nonlinearity, dispersion, and higher-order quantum effects introduced by the Bohm potential in shaping solitonic structure. Moreover, the reported analytical structures are qualitatively consistent with experimentally observed soliton propagation in nonlinear optical fibers and photonic guiding media, which supports the practical relevance of the present theoretical model. This work opens several promising directions for future investigation. In particular, a natural extension of the present study is to examine the stability and perturbation dynamics of the obtained soliton solutions through linear stability analysis and numerical simulations. Such investigations would provide deeper insight into the robustness of the derived wave structures under small disturbances and realistic physical conditions. Furthermore, exploring fractional-order or variable-coefficient versions of the RNLSE may reveal additional dynamical features associated with memory effects and inhomogeneous nonlinear media. The inclusion of gain–loss mechanisms and the study of higher-dimensional extensions of the model could further broaden its applicability in areas such as photonic crystal waveguides, nonlinear plasmonics, and optical signal processing. Finally, numerical simulations based on the obtained analytical solutions may help validate the theoretical predictions and support potential experimental realizations in nonlinear optics and quantum technologies.

Declarations

Conflict of interest

The authors declare that they have no conflict of interest.

Data availability

No data was used or generated in the paper.

Funding

Princess Nourah bint Abdulrahman University Researchers Supporting Project number (PNURSP2026R443), Princess Nourah bint Abdulrahman University, Riyadh, Saudi Arabia.

Acknowledgment

Princess Nourah bint Abdulrahman University Researchers Supporting Project number (PNURSP2026R443), Princess Nourah bint Abdulrahman University, Riyadh, Saudi Arabia.

References

[1] El-Shorbagy M A, Akram S and Rahman M ur 2024 Partial Differ. Equ. Appl. Math. 12 100955

[2] Eskandari Z, Avazzadeh Z, Ghaziani R K and Li B 2025 Math. Methods Appl. Sci. 48 7197.

[3] Akram S, Rahman M ur and Al-Essa L A 2025 High Energy Density Phys. 57 101234.

[4] Li B, Zhang Y, Li X, Eskandari Z and He Q 2023 J. Comput. Appl. Math. 426 115089.

[5] Karjanto N 2024 Mathematics 12 744.

[6] El-Shorbagy M A, Akram S and Rahman M ur 2024 Partial Differ. Equ. Appl. Math. 12 100955.

[7] Du W, He Q, Cao T and Wu J 2025 Oper. Res. Lett. 107367.

[8] Hossain M N, Miah M M, Ganie A H, Osman M S and Ma W X 2024 Opt. Quantum Electron. 56 847.

[9] Rahman M ur and Akram S 2026 J. Appl. Anal. Comput. 16 1668.

[10] Zhang X, Yang X and He Q 2022 N. Am. J. Econ. Finance 62 101766.

[11] Hamali W, Manafian J, Lakestani M, Mahnashi A M and Bekir A 2024 Opt. Quantum Electron. 56 7.

[12] Wang K J and Li S 2024 Europhys. Lett. 146 62003.

[13] Iqbal M A, Hussain M, Safeer M, Taj M and Tounsi A 2025 Comput. Concr. 35 155.

[14] Alsisi A 2024 Alex. Eng. J. 99 31.

[15] Shahid N, Baber M Z, Shaikh T S, Iqbal G, Ahmed N, Akgul A and De la Sen M 2024 Results Phys. 58 107444.

[16] Murad M A S 2024 J. Opt. 1.

[17] Ashraf F, Ashraf R and Akgul A 2024 Int. J. Mod. Phys. B 38 2450329.

[18] Haider J A, Alhuthali A M S and Elkotb M A 2024 Results Phys. 60 107684.

[19] Farooq A, Khan M I and Ma W X 2024 Opt. Quantum Electron. 56 542.

[20] Alquran M, Jaradat I, Momani S and Baleanu D 2020 Rom. Rep. Phys. 72 117.

[21] Korsunsky S V 1994 Phys. Lett. A 185 174.

[22] Ozisik M, Secer A, Bayram M, Cinar M, Ozdemir N, Esen H and Onder I 2023 Optik 274 170548.

[23] Zhu X, Xia P, He Q, Ni Z and Ni L 2023 Int. J. Bio-Inspired Comput. 21 106.

[24] Rahman M ur and Akram S 2026 Z. Naturforsch. A.

[25] Yang J 2010 Nonlinear Waves in Integrable and Nonintegrable Systems (SIAM).

[26] Kivshar Y S and Agrawal G P 2003 Optical Solitons: From Fibers to Photonic Crystals (Academic Press).

[27] Hirota R and Satsuma J 1981 Phys. Lett. A 85 407.

[28] Wazwaz A M 2018 Alex. Eng. J. 57 1971.

[29] Wazwaz A M 2017 Math. Methods Appl. Sci. 40 4128.

[30] Wazwaz A M 2017 Math. Methods Appl. Sci. 40 4128.

[31] Jaradat H M 2018 Alex. Eng. J. 57 2151.

[32] Syam M, Jaradat H M and Alquran M 2017 Nonlinear Dyn. 90 1363.

[33] Alquran M, Jaradat H M and Syam M I 2018 Nonlinear Dyn. 91 1619.

[34] Alquran M and Jarrah A 2019 J. King Saud Univ. Sci. 31 485.

[35] Yassin O and Alquran M 2018 Appl. Math. Inf. Sci. 12 361.

[36] Jaradat I, Alquran M, Momani S and Biswas A 2018 Optik 172 822.

[37] Alquran M and Jaradat I 2019 Nonlinear Dyn. 96 115.

[38] Abu Irwaq I, Alquran M, Jaradat I and Baleanu D 2018 Adv. Differ. Equ. 433.

[39] Dokuyucu M A, Celik E, Bulut H and Baskonus H M 2018 Eur. Phys. J. Plus 133 92.

[40] Chou D, Tariq K U, Rehman H U and Rashid A 2025 Math. Methods Appl. Sci.

[41] Nuruddeen R I, Aboodh K S and Ali K K 2020 J. King Saud Univ. Sci. 32 677.

[42] Ozisik M, Bayram M, Secer A and Cinar M 2024 Eur. Phys. J. Spec. Top. 233 1331.

[43] Kadkhoda N 2017 Int. J. Appl. Comput. Math. 3 1415.

[44] Mollenauer L F, Stolen R H and Gordon J P 1980 Phys. Rev. Lett. 45 1095.

[45] Hasegawa A and Tappert F 1973 Appl. Phys. Lett. 23 142.

[46] Kivshar Y S and Agrawal G P 2003 Optical Solitons: From Fibers to Photonic Crystals (San Diego: Academic Press).